Journal of Sound and Vibration 641 (2026) 119904

Contents lists available at ScienceDirect

Journal of Sound and Vibration

journal homepage: www.elsevier.com/locate/jsvi

Pedestrian-sensed indirect footbridge frequency identification

Zhenkun Li [a,*], Suzana Ereiz [a], Ekin Ozer [b,c], Abdollah Malekjafarian [b,d], Maria Pina Limongelli [a]

[a] Department of Architecture, Built Environment and Construction Engineering, Politecnico di Milano, 20133, Milano, Italy
[b] School of Civil Engineering, University College Dublin, D04 V1W8, Dublin, Ireland
[c] UCD Earth Institute, University College Dublin, D04 V1W8, Dublin, Ireland
[d] Structural Dynamics and Assessment Laboratory, School of Civil Engineering, University College Dublin, D04 V1W8, Dublin, Ireland

ARTICLE INFO

Keywords:
Structural health monitoring
Pedestrian–structure interaction
Footbridges
Frequency identification
Crowdsensing

ABSTRACT

While indirect bridge monitoring has been widely investigated using vehicles and, more recently, micromobility devices, the use of pedestrian response for footbridge frequency identification has yet to be systematically studied. To fill this gap, this paper proposes a new pedestrian-sensed indirect monitoring method for identifying the natural frequencies of footbridges, in which pedestrians themselves serve as low-cost moving sensors rather than requiring a dedicated sensing system on the footbridge. The key novelty lies in demonstrating the feasibility of extracting footbridge modal information directly from pedestrian vibration responses under various pedestrian activities. Numerical simulations of pedestrian–footbridge interaction are carried out for three representative activities, namely standing, jumping, and walking, to examine the feasibility of capturing footbridge modal information in pedestrian responses. The results show that footbridge frequencies can be observed from pedestrian vibrations in all three scenarios. The high damping of pedestrians suppresses their own frequencies, which helps highlight footbridge frequencies, with the pedestrian acting as a weak "low-pass filter". For walking cases, both footbridge frequencies and walking excitation frequencies appear in the pedestrian response, and the higher footbridge frequencies exhibit a "camel hump phenomenon" due to the moving-sensor effect. Finally, the influences of pedestrian mass, walking speed, environmental noise, footbridge frequency, and footbridge damping are investigated to assess the robustness and limitations of the proposed method.

1. Introduction

Structural health monitoring (SHM) of bridges has become an important research topic since the early 21st century [1]. A key reason is that many bridges worldwide were built after the 1950s and have now been in service for more than 70 years. Over the past two decades, issues of aging and deterioration have become increasingly evident. Reports from the EU and the U.S. indicate that a significant proportion of bridges are in poor condition [2,3]. At the same time, new bridges are continually being constructed and require reliable monitoring throughout their service life. Consequently, stakeholders and bridge owners are actively seeking effective solutions to assess the condition of these structures, inform maintenance decisions, optimize investments, and prevent failures or collapses. In recent years, vibration-based methods have shown considerable promise for SHM [4–6].

* Corresponding author.
E-mail addresses: zhenkun.li@polimi.it, zhenkun-li@outlook.com (Z. Li), suzana.ereiz@polimi.it (S. Ereiz), ekin.ozer@ucd.ie (E. Ozer), abdollah.malekjafarian@ucd.ie (A. Malekjafarian), mariagiuseppina.limongelli@polimi.it (M.P. Limongelli).

https://doi.org/10.1016/j.jsv.2026.119904
Received 15 January 2026; Received in revised form 18 May 2026; Accepted 19 May 2026
Available online 20 May 2026

The most straightforward approach to vibration-based SHM is to install accelerometers directly on the target bridges to collect structural health data [7] (referred to as the direct method in this work). Researchers have investigated variations of modal parameters, such as natural frequencies, mode shapes, and damping ratios, identified from bridge vibrations, which can serve as indicators for damage detection [8]. To distinguish variations caused by structural damage from those arising due to environmental and operational conditions, various methods have been proposed, including input–output and output-only models that incorporate environmental measurements to mitigate these effects [9]. These studies highlight the fundamental role of modal parameters in bridge health monitoring [10]. However, several practical challenges remain. First, this approach typically requires installing sensors on a bridge to capture its condition, rendering it costly [11,12]. Second, the approach lacks transferability, as it generally applies to a single bridge, limiting its scalability for network-level monitoring across a region [13]. Finally, because of the high costs, such methods are usually reserved for large or critical bridges, leaving footbridges largely unmonitored, despite playing a vital role in urban and global transportation networks [14,15].

To reduce monitoring costs and simplify procedures, the indirect method (also known as the drive-by method or vehicle scanning method [16,17]) was proposed and demonstrated through numerical simulations in 2004 [18]. The effectiveness of the proposed method was demonstrated by field tests in the following year [19]. In this approach, accelerometers are mounted on vehicles instead of bridges, which significantly lowers costs. Since then, the method has been gradually developed and studied through numerical simulations [20], laboratory experiments [21], and full-scale tests [22]. Foundational studies focus on extracting bridge frequencies from the responses of passing vehicles, providing a basis for further investigation. Nonetheless, similar to direct SHM methods, the drive-by method has mainly been applied to road bridges rather than footbridges. This limitation arises because conventional vehicles are not permitted on footbridges, thereby restricting the applicability of the indirect approach.

To address the above limitation, researchers have recently explored the use of micromobility devices for extracting road/footbridge modal information and performing health monitoring [23,24]. In 2022, Quqa et al. [25] proposed using shared bicycles to identify the modal parameters of a footbridge in Bologna, Italy. A smartphone was mounted on a bicycle to record vibrations during crossings. To reduce the influence of road roughness, the bicycle was ridden at a relatively low speed and repeated traversals were carried out to minimize uncertainties. A band-pass filter was applied to remove bicycle-related frequencies. Field test results demonstrated that this method could successfully identify the fundamental frequency and operational modes of the footbridge. However, the approach required pedaling, which introduced additional vibration components due to human pedaling forces. In 2024, May et al. [26] used a smartphone attached to a bicycle to determine the fundamental frequency of a footbridge, while also installing sensors directly on the bridge for validation. Furthermore, factors such as rider posture and pedaling cadence affect the effective frequency of the rider–bicycle system, potentially causing non-stationary frequency variations in the combined rider–bicycle–bridge system. To eliminate the influence of pedaling, researchers began investigating electric scooters. McSweeney et al. [27] attached smartphones to both the scooter deck and the footbridge to identify bridge frequencies. They found that the first frequency obtained from scooter measurements was approximately 0.5 Hz lower than that measured on the bridge, attributable to the driving frequency of the electric scooter, which depends on the vehicle's speed and the bridge span. Although micromobility response can provide valuable information, such as modal frequencies and other damage indicators, several challenges remain.

Some footbridges prohibit bicycles or scooters, limiting the applicability of micromobility-based methods and motivating monitoring approaches that rely solely on pedestrians. Moreover, smartphones are not originally part of micromobility systems, so they must be externally attached. All of these factors make the monitoring of footbridges challenging. Furthermore, because the footbridge and micromobility vehicle are connected through tires, road roughness continues to strongly influence the recorded response and may significantly hinder the accurate extraction of bridge information. Previous studies on footbridges have extensively investigated pedestrian–structure interaction (PSI) and vibration mitigation strategies, including semi-active control considering human–structure interaction, adaptive-passive tuned mass dampers with variable stiffness, and semi-active tuned mass dampers under random crowd-induced vibration including crowd–structure interaction [28–30]. However, the use of pedestrian response for structural health monitoring has rarely been studied (e.g., Ozer and Feng [31]). That study was experimental and non-parametric, lacked damping observations, and represented pedestrian biomechanics in a rather simplistic manner via transfer functions. However, the use of wearable sensors on human beings for different purposes, such as fall detection and other human activity recognition [32,33], have been well studied. Responses recorded by smartphones or other wearable sensors have great potential to become an important component of crowdsensing-based infrastructure health monitoring in the near future [34–36].

To address these challenges while leveraging the opportunities offered by crowdsensing, this study proposes using the response of pedestrians as mobile sensors for identifying the natural frequencies of footbridges. The main novelties and contributions of this study are summarized as follows. Unlike previous studies mainly focusing on PSI for response prediction, serviceability assessment, or vibration mitigation through control devices, the present work investigates whether the pedestrian response itself can be used as an information carrier for indirect footbridge frequency identification. In this sense, the pedestrian is treated not only as an excitation source that interacts with the structure, but also as a mobile carrier of structural vibration information. More specifically, this work makes the following contributions: (1) it proposes a pedestrian-sensed indirect frequency identification concept for footbridges without requiring dedicated bridge-mounted sensors; (2) it systematically examines the feasibility of extracting footbridge frequencies from pedestrian vibrations under standing, jumping, and walking conditions; and (3) it clarifies the key transfer mechanisms and limitations of the proposed approach, including the filtering effect of pedestrian dynamics, the coexistence of walking harmonics and footbridge frequencies, and the influence of several practical factors, as examined through parametric studies. The key advantage of this approach is that it does not require dedicated sensing systems installed on the footbridge or specialized equipment. In practical implementation, the pedestrian response can be measured using built-in inertial sensors in smartphones or lightweight wearable devices already carried during normal bridge usage. Therefore, the proposed approach does not require dedicated bridge-mounted

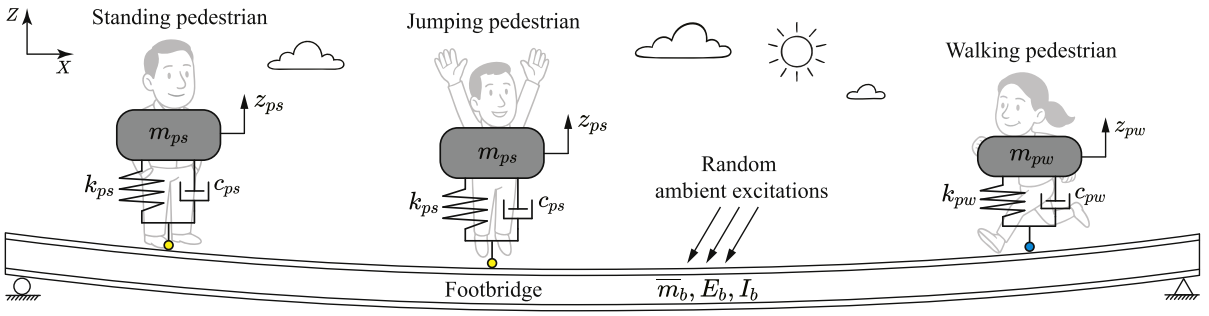

Fig. 1. Pedestrians on the footbridge.

instrumentation but instead relies on opportunistic measurements from ordinary pedestrians, that is, during their normal use of the footbridge rather than during a dedicated test. The proposed approach is not intended to replace direct measurements. Instead, the main objective is to explore whether ordinary pedestrians during normal bridge usage can act as movable sensors for opportunistic footbridge monitoring. This makes the method particularly attractive for low-cost, rapid, and scalable screening of footbridges, where dedicated instrumentation is often unavailable or difficult to employ.

The remainder of this paper is organized as follows. Section 2 presents the PSI model and the theoretical foundation of the proposed approach. Section 3 describes the numerical simulations, covering three scenarios and their corresponding analysis results and discussions. Section 4 investigates the sensitivity of the proposed method to various parameters. Finally, Section 5 provides the conclusions and outlines directions for future research.

2. Theory

This section presents the basic theory proposed for identifying footbridge frequencies using pedestrian vibration response. The pedestrian models, the footbridge model, and their interaction model are described in detail. Pedestrians typically perform various activities on footbridges. In this study, three representative activities, namely standing, jumping, and walking/running, are considered and the relevant pedestrian models are introduced in the following subsections together with the employed footbridge model.

2.1. Pedestrian models

Three pedestrian models corresponding to the activities of standing, jumping, and walking/running, as shown in Fig. 1, are presented as follows.

2.1.1. Standing pedestrian

Standing is a common pedestrian posture on footbridges, during which bridge vibrations are transmitted to the pedestrian through the PSI mechanism. In practice, the response data could be collected opportunistically via a smartphone application, transmitted automatically without requiring any sensors on the footbridge itself. In this study, the standing pedestrian interacting with the structure is modeled as a single-degree-of-freedom damped spring-mass system, as shown in Eq. (1) [37],

$$m_{ps} = 1.03M_p, k_{ps} = 1340M_p, c_{ps} = 51.6M_p, \tag{1}$$

where M_p is the static mass of the pedestrian, and m_{ps}, k_{ps}, and c_{ps} represent the mass, stiffness, and damping of the pedestrian's biomechanical model, respectively. The coefficients, such as 1.03, 1340, and 51.6, are determined by fitting to experimental data of standing pedestrians. When the pedestrian is in the standing posture, environmental and operational excitations are the main sources exciting the footbridge. Although passing micromobility vehicles and other walking pedestrians can introduce additional energy to the footbridge and increase its vibration amplitude, such excitations are not continuously available. Therefore, in this study, only random ambient excitations applied to the footbridge are considered.

2.1.2. Jumping pedestrian

Sometimes, pedestrians may jump on the footbridge. Unlike standing pedestrians, jumping pedestrians can actively apply excitation to the footbridge, causing stronger vibrations. The jumping force can be represented as the sum of two Gaussian functions [38], as shown in Eq. (2),

$$F_{pj}(t) = \sum_{i=1}^{2} A_i \cdot \exp(-((t - t_i)^2/2b_i^2)), t \in [0, T], \tag{2}$$

where $A_i = \alpha_i^j M_p g$ denotes the height of the ith Gaussian peak, and g is the gravitational acceleration ($g = 9.81\,\mathrm{m/s^2}$). $T = 1/f_{pj}$ represents the duration of one jumping cycle, with f_{pj} being the jumping frequency. t_i is the center position of the ith peak, and

Table 1
Parameters for jumping force simulation [38].

Parameter	α_1^j	$b_1(s)$	$t_1(s)$	α_2^j	$b_2(s)$	$t_2(s)$
Value	2.795	0.07	0.232	1.4588	0.06	0.306

Table 2
Parameters of walking/running pedestrians [42].

Parameter	Slow walk	Normal walk	Fast walk	Jogging
Pacing frequency f_{pw}^p (Hz)	1.7	2.0	2.3	2.5
Forward speed v_{pw} (m/s)	1.1	1.5	2.2	3.3

b_i controls the width, that is, the time duration of the corresponding bell-shaped curve. This term represents an impact-like force generated during each pedestrian jump. The time duration of this curve describes how long this force is effectively applied to the footbridge. Physically, it reflects the contact time and the compliance or stiffness of the landing. According to Ref. [38], for 44 consecutive jumping cycles, the mathematical model with the parameters listed in Table 1 provides a good fit for the experimental results. Therefore, these parameters are adopted in this study to simulate the jumping force. After completing the jump, it is assumed that the pedestrian stands still on the footbridge, returning to the condition described in Section 2.1.1. Consequently, the same biomechanical model used for standing pedestrians is applied for further analysis.

2.1.3. Walking/running pedestrian

The third common activity performed by pedestrians is walking or running, which can be distinguished based on their pacing frequency and forward speed. A practical approach to modeling a walking pedestrian is to represent the pedestrian as a damped spring–mass system (different from the standing or jumping models) that moves along the structure while simultaneously applying the excitation force generated during walking/running on a rigid surface [39].

When a pedestrian walks or runs on a footbridge, the parameters of their biomechanical model can be described using approximate nonlinear functions, as shown in Eq. (3) [40].

$$\begin{aligned} m_{pw} &= 97.082 + 0.275M_p - 37.518f_{pw}^p, \\ c_{pw} &= 29.041m_{pw}^{0.883}, \\ k_{pw} &= 30351.744 - 50.261c_{pw} + 0.035c_{pw}^2, \end{aligned} \tag{3}$$

where f_{pw}^p is the pedestrian's pacing frequency, and m_{pw}, c_{pw}, and k_{pw} represent the mass, damping, and stiffness of the pedestrian biomechanical model, respectively. These equations are empirical biomechanical models, and the numerical coefficients come from regression fitting to experimental PSI data in Ref. [40]. In m_{pw}, the constants represent a baseline dynamic mass and the associated scaling factor. Only a fraction of the body mass contributes to vertical vibration, and the effective mass decreases with pacing frequency because faster walking reduces how much of the body moves coherently with the structure. In c_{pw}, the coefficient and exponent describe how human energy dissipation scales with the effective moving mass. The sublinear exponent reflects that damping increases with mass, but not proportionally. In k_{pw}, stiffness is expressed as a function of damping because both are governed by muscle activation and joint control. The numerical terms capture the experimentally observed nonlinear coupling between damping and stiffness during walking. Meanwhile, the excitation force generated by a walking or running pedestrian can be expressed as a sum of their Fourier harmonic components [41], as shown in Eq. (4).

$$F_{pw}(t) = M_p g + \sum_{i=1}^{n} M_p g \alpha_i^w \sin\left(2\pi i f_{pw}^p t - \phi_i^w\right), \tag{4}$$

where α_i^w is the Fourier coefficient of the ith harmonic, ϕ_i is the corresponding phase angle, and n denotes the total number of contributing harmonics. Specifically, for pedestrians walking on a footbridge [42], α_i^w and ϕ_i^w can be assigned as follows: $\alpha_1^w = 0.4$, $\alpha_2^w = \alpha_3^w = 0.1$, and $\phi_1^w = 0$, $\phi_2^w = \phi_3^w = \pi/2$. These values are taken from experimental studies based on Fourier analysis of measured pedestrian walking forces. The number of harmonics n is taken as 3. This choice is justified because the first three harmonics capture nearly all dynamically relevant content of pedestrian walking forces and ignoring higher-order harmonics has a negligible effect on walking force simulations. In addition, to account for diverse pedestrian conditions, several values of the pacing frequency f_{pw}^p and walking/running speed v_{pw} are considered and summarized in Table 2.

The pedestrian models for the activities described above are all damped spring-mass systems with varying parameters. Their dynamic equilibrium equations can be expressed in a unified form, as shown in Eq. (5),

$$m_p \ddot{z}_p(t) + c_p \dot{z}_p(t) + k_p z_p(t) = F_p'(t), \tag{5}$$

where m_p represents m_{ps} for standing or jumping pedestrians and m_{pw} for walking/running pedestrians, as shown in Fig. 1. Similarly, k_p and c_p denote the corresponding pedestrian stiffness and damping. The symbols z_p, $\dot{z}_p$, and $\ddot{z}_p$ denote the displacement, velocity, and acceleration of the lumped mass of the pedestrian model. $F_p'(t)$ is the contact force applied to the pedestrian from the interaction point between the pedestrian and footbridge.

2.2. Footbridge model

The footbridge in this study is modeled as a simply supported Euler–Bernoulli beam. It is divided into N' elements, characterized by a mass per unit length $\overline{m}_b$, Young's modulus E_b, and moment of inertia I_b. The total length of the footbridge is L. All nodes except for the supporting ends have two degrees of freedom: vertical translation and rotation, while the supporting ends only have one degree of freedom: rotation. The dynamic equilibrium equation of the footbridge can be expressed as Eq. (6),

$$\mathbf{M}\ddot{\boldsymbol{z}}^N(t) + \mathbf{C}\dot{\boldsymbol{z}}^N(t) + \mathbf{K}\boldsymbol{z}^N(t) = \boldsymbol{p}^N(t), \tag{6}$$

where $\mathbf{M}$, $\mathbf{C}$, and $\mathbf{K}$ are the mass, damping, and stiffness matrices of the footbridge's finite element model. Here, $\boldsymbol{p}^N(t)$ denotes the total external force vector applied to the footbridge finite element model. In the present study, it is composed of the ambient excitation and the pedestrian-related contact force, as shown in Eq. (7),

$$\boldsymbol{p}^N(t) = \boldsymbol{p}_{\text{amb}}(t) + \mathbf{L}_c(t) \cdot F_c(t), \tag{7}$$

where $\boldsymbol{p}_{\text{amb}}(t)$ is the ambient excitation vector, $\mathbf{L}_c(t)$ is the location vector that maps the contact force to the adjacent degrees of freedom of the bridge using the Hermitian cubic interpolation function [43], and $F_c(t)$ is the vertical force acting at the pedestrian–footbridge contact point. For the standing case, $F_c(t) = F'_p(t)$; for the jumping case, $F_c(t) = F'_p(t) + F_{pj}(t)$; and for the walking case, $F_c(t) = F'_p(t) + F_{pw}(t)$, where $F_{pj}(t)$, and $F_{pw}(t)$ are defined in Eqs. (2) and (4), respectively, while $F'_p(t)$ will be introduced in the following section. The displacement, velocity, and acceleration vectors at all degrees of freedom are denoted as $\boldsymbol{z}^N$, $\dot{\boldsymbol{z}}^N$, and $\ddot{\boldsymbol{z}}^N$. In this study, Rayleigh damping is assumed, which is modeled as $\mathbf{C} = \alpha_0\mathbf{M} + \beta_0\mathbf{K}$. If the first two damping ratios, ξ_1 and ξ_2, are both assumed to be ξ, the damping ratio assigned to both modes, the Rayleigh damping coefficients α_0 and β_0 can be determined from Eq. (8), in which $\omega = 2\pi f$ is the angular frequency in rad/s [44].

$$[\alpha_0, \beta_0] = 2\xi \cdot [\omega_{b1}\omega_{b2}, 1]/(\omega_{b1} + \omega_{b2}) \tag{8}$$

2.3. Interaction between the pedestrian and footbridge

This study adopts a separate modeling approach for the pedestrian and the footbridge [45], in which the governing equations are solved using an uncoupled iterative procedure. In the literature related to vehicle-bridge interaction, such algorithms are generally classified into two categories: (1) uncoupled iterative procedures, in which the equations of motion of the two subsystems are solved separately and compatibility at the contact point is enforced iteratively, and (2) coupled-system formulations, in which a unique system matrix is formed and solved at each time step. In this study, the former strategy is adopted because it is straightforward to implement, computationally efficient, and compatible with separate pedestrian and footbridge models. Three scenarios are investigated: standing, jumping, and walking pedestrians. In all cases, random ambient excitations are also applied to the footbridge. Such random excitations may arise from wind, nearby traffic, surrounding pedestrian activity, ground vibration, and other environmental or operational sources. Including such excitations helps simulate more realistic conditions in engineering applications. The interaction process is described as follows.

Initially, the vibration response of both the pedestrian and the footbridge is set to zero. External excitations are then applied to the footbridge nodes to induce vibrations. Specifically, for a standing pedestrian, only ambient excitations are considered, whereas for a jumping pedestrian, the excitation also includes the jumping force defined in Eq. (2). For walking pedestrians, the walking force described by Eq. (4) is applied along the footbridge as the pedestrian moves. The footbridge vibrations are computed using the Newmark–β integration method, where $\beta = 0.25$ and $\gamma = 0.5$ are adopted to ensure unconditional stability [46]. However, the footbridge vibrations, in turn, influence the pedestrian's response. Therefore, based on the calculated footbridge vibrations, the contact force applied to the pedestrian can be obtained by Eq. (9),

$$F'_p(t) = k_p \cdot (z_p(t) - u_c(t)) + c_p \cdot (\dot{z}_p(t) - \dot{u}_c(t)), \tag{9}$$

where k_p and c_p are the same as those defined in Eq. (5). The symbols u_c and $\dot{u}_c$ represent the displacement and velocity response of the footbridge at the contact point(s) between the pedestrian and the footbridge. At this stage, $z_p(t) = 0$ and $\dot{z}_p(t) = 0$. Using Eq. (5) together with the Newmark–β integration method, the pedestrian's vibration response can be obtained. With the updated pedestrian response, the excitation applied to the footbridge is recalculated by summing the interaction force $F'_p(t)$, the ambient excitations, and the jumping/walking force. The footbridge response is updated accordingly. By repeating this iterative process, the difference between the excitations applied to the footbridge in two consecutive iterations gradually decreases and converges to a small threshold value, herein assumed as 10^{-2} N. Once convergence is achieved, the iterations are terminated, and the coupled vibration response of the pedestrian and footbridge is obtained. This procedure corresponds to an uncoupled iterative interaction algorithm, in which the pedestrian and footbridge responses are solved separately and the interaction force is updated iteratively until convergence [47]. This type of formulation is widely used in engineering applications because it facilitates implementation and avoids the need to update a fully coupled system matrix at every time step.

A fully coupled PSI formulation could alternatively be established by assembling the pedestrian and footbridge degrees of freedom into a single system matrix [48,49]. Such an approach is rigorous from a system-level viewpoint, but it generally requires updating the global system matrix as the interaction point changes with time, which may increase computational effort. Therefore, for the present proof-of-concept study, the uncoupled iterative formulation was considered more suitable.

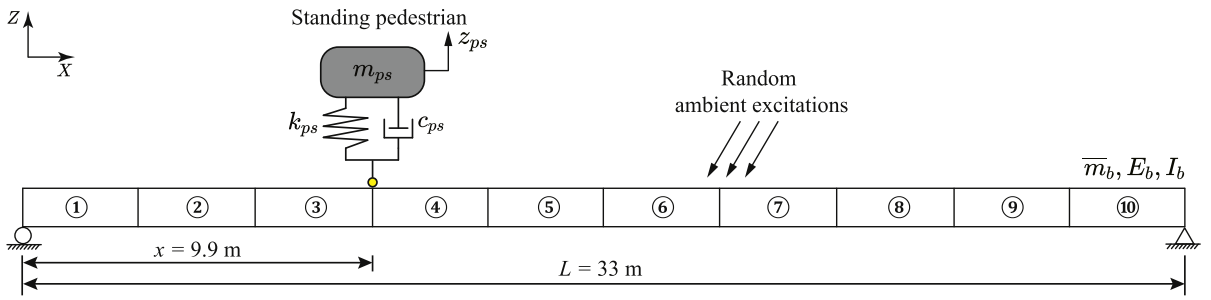

Fig. 2. Pedestrian standing on the footbridge.

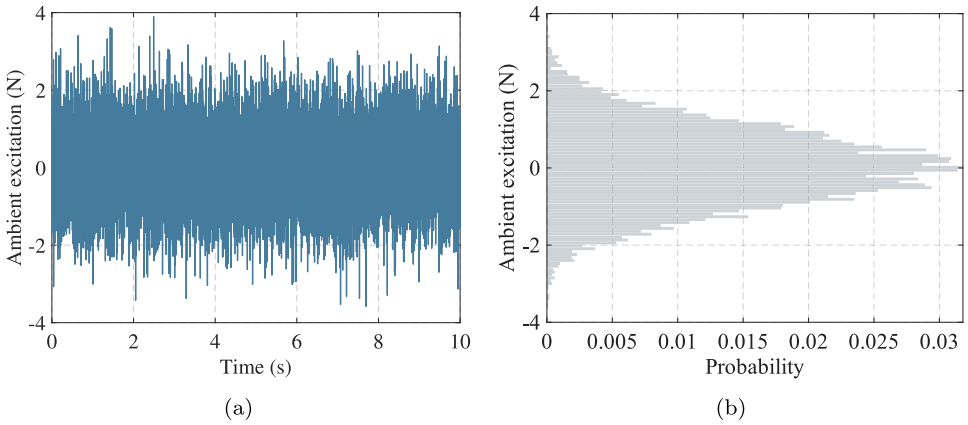

Fig. 3. Ambient excitations on one node of the footbridge: (a) ambient excitation; (b) histogram of the excitation.

3. Simulation results and discussions

This section presents case studies corresponding to several scenarios based on the proposed method described in Section 2. It first introduces the parameters used for the pedestrian and footbridge models, followed by the results and discussion on footbridge frequency identification.

3.1. Parameters

In this study, the static mass of a pedestrian is assumed to be $M_p = 60\,\text{kg}$, representing an individual performing various activities on the footbridge. According to Eq. (1), the parameters for the standing posture are determined as $m_{ps} = 6.18 \times 10^1\,\text{kg}$, $c_{ps} = 3.096 \times 10^3\,\text{N}\cdot\text{s/m}$, and $k_{ps} = 8.04 \times 10^4\,\text{N/m}$. For the walking posture, the pedestrian is assumed to walk at a normal pace with a pacing frequency of $f_{pw}^p = 2.0\,\text{Hz}$. Using Eq. (3), the corresponding parameters are obtained as $m_{pw} = 3.855 \times 10^1\,\text{kg}$, $c_{pw} = 7.302 \times 10^2\,\text{N}\cdot\text{s/m}$, and $k_{pw} = 1.231 \times 10^4\,\text{N/m}$.

The footbridge parameters are estimated based on a real structure reported in Ref. [14]. Although detailed model updating is not performed, the model captures the key characteristics of the primary girders of the real footbridge. The parameters of the footbridge are as follows: $L = 33\,\text{m}$, flexural stiffness $E_b I_b = 1.389 \times 10^9\,\text{N}\cdot\text{m}^2$, and mass per unit length $\overline{m}_b = 224\,\text{kg/m}$. The beam model of the footbridge is divided into 10 elements ($N' = 10$), as shown in Fig. 2. Damping is initially neglected to provide a clear baseline for validating the proposed method and is then examined in detail in Section 4.5.

Based on the above parameters, the natural frequency of the standing pedestrian is calculated as $f_{ps} = 5.741\,\text{Hz}$, while that of the walking pedestrian is $f_{pw} = 2.845\,\text{Hz}$. For the footbridge, the first three natural frequencies are $f_{b1} = 3.593\,\text{Hz}$, $f_{b2} = 14.373\,\text{Hz}$, and $f_{b3} = 32.353\,\text{Hz}$. Three scenarios, standing, jumping, and walking/running pedestrians, are investigated to validate the proposed method. The sampling frequency is set to 100 Hz, which corresponds to the maximum sampling frequency achievable by most smartphones [14,25].

3.2. Scenario 1: standing

When standing, the footbridge is stimulated only by ambient excitations, and the bridge information is transferred to the pedestrian via the PSI process. In this study, the pedestrian is assumed to stand at a position $x = 9.9\,\text{m}$ from the left end of the footbridge, as shown in Fig. 2.

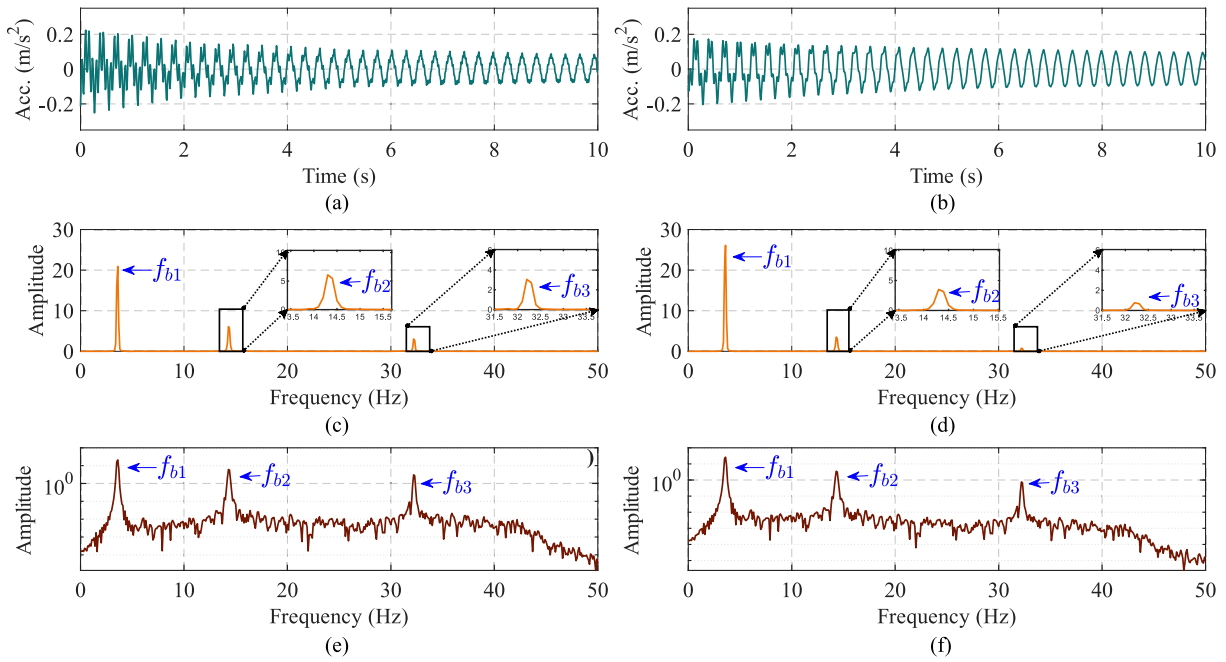

Fig. 4. Accelerations and frequency spectra of the footbridge and standing pedestrian: (a) footbridge acceleration; (b) pedestrian acceleration; (c) footbridge frequency spectrum in linear scale; (d) pedestrian frequency spectrum in linear scale; (e) footbridge frequency spectrum in log scale; (f) pedestrian frequency spectrum in log scale.

At the same time, a random ambient excitation f_i^N following a normal distribution, $f_i^N \sim \mathcal{N}(0,1)$, is applied to each vertical degree of freedom of the footbridge, representing a Gaussian white-noise input [50]. In the numerical simulation, this excitation is independently generated at each time step and serves as a simplified broadband representation of low-level environmental and operational disturbances, such as wind effects, surrounding pedestrian activity, and other minor ambient sources. The zero mean ensures that no directional bias is introduced, while the unit variance provides a normalized stochastic input level for the feasibility study. The main purpose of this excitation is to excite the footbridge over a broad frequency range so that the transfer of bridge modal information to the pedestrian response can be examined. Fig. 3a shows an example of the vertical ambient excitation at the standing point. Fig. 3b shows the histogram of the ambient excitation signal at the same position. The distribution is approximately symmetric about zero and follows the bell-shaped trend expected from a Gaussian random process. This indicates that positive and negative excitation values occur with similar probability and confirms that the generated signal is consistent with the assumed normal distribution used in the simulation.

Fig. 4 presents 10 seconds of the vibration response in terms of acceleration time histories (a and b) and frequency spectra (c–f) of both the footbridge and the standing pedestrian. The two time histories show strong resemblance. Initially, the acceleration amplitude of the footbridge is slightly higher than that of the pedestrian. However, once the signals stabilize, the pedestrian's vibration response is smoother than that of the footbridge.

A Hanning window is applied prior to performing the Fast Fourier Transform (FFT) to minimize spectral leakage in the computation of the frequency spectra, which are displayed on both linear and logarithmic scales, as shown in Fig. 4c–f. The first three natural frequencies of the footbridge are clearly identified in both the footbridge and pedestrian responses under ambient excitation. However, the amplitudes corresponding to the second and third frequencies are relatively low. Moreover, the amplitude of the first natural frequency is higher in the pedestrian response than in the footbridge response, whereas the amplitudes of the second and third frequencies are lower in the pedestrian response. Under this condition, these results indicate that the standing pedestrian behaves as a weak "low-pass filter," attenuating the footbridge response in the higher frequency range.

The pedestrian's natural frequency cannot be identified from the pedestrian response frequency spectrum shown in Fig. 4d and f. To further investigate this phenomenon, a reduced pedestrian damping value $\bar{c}_{ps}$ is considered. The variation of the spectral amplitude with respect to the ratio $\bar{c}_{ps}/c_{ps}$ and frequency is presented in Fig. 5. In this analysis, the pedestrian mass and stiffness are kept constant. Therefore, the pedestrian natural frequency f_{ps} does not change. Only the damping coefficient is gradually reduced by scaling the ratio $\bar{c}_{ps}/c_{ps}$. It can be observed that for realistic damping levels, the pedestrian's own natural frequency is strongly attenuated and does not appear in the spectrum, whereas the footbridge frequency f_{b1} remains clearly identifiable. As the damping is artificially reduced, a resonance peak gradually emerges at f_{ps}, while the amplitude of f_{b1} remains nearly unchanged. This demonstrates that the high damping of the pedestrian suppresses its own resonance and facilitates effective transfer of footbridge vibrations without spectral interference.

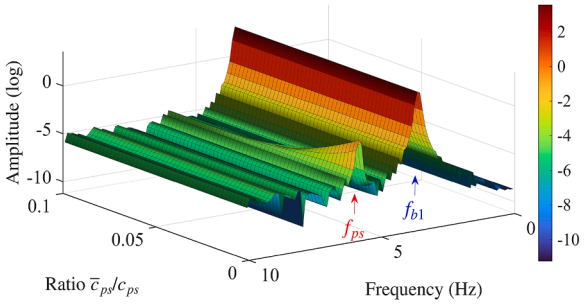

Fig. 5. Effects of pedestrian damping.

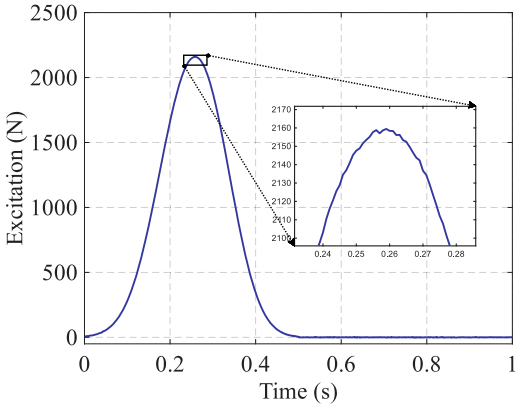

Fig. 6. Jumping and ambient excitations.

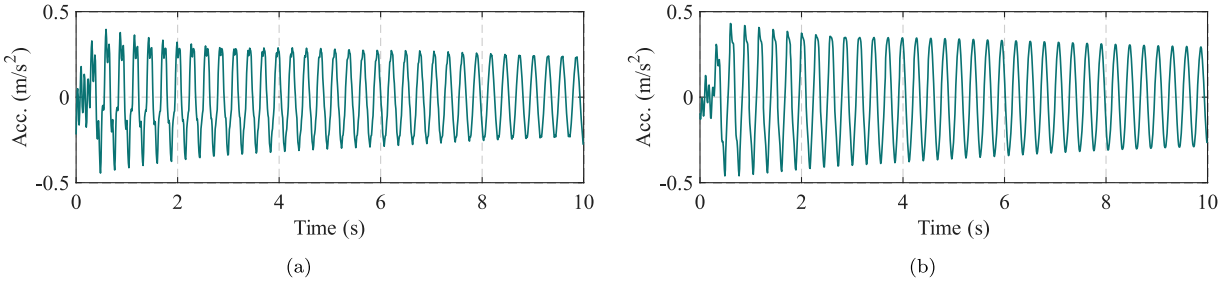

Fig. 7. Accelerations of the footbridge and jumping pedestrian: (a) footbridge; (b) pedestrian.

3.3. Scenario 2: jumping

In this scenario, the pedestrian performs a single jump at the same location as in Scenario 1, namely $x = 9.9$ m from the left support, and then remains standing on the footbridge. Therefore, the jumping case consists of two successive stages: an initial short-duration active excitation stage, during which the jumping force defined in Eq. (2) is applied, and a subsequent passive interaction stage, during which the pedestrian behaves as the standing biodynamic model described in Section 2.1.1. In addition to the random ambient excitation, the jumping force is applied during the interval 0–0.5 s. As shown in Fig. 6, the total excitation at the jumping point is dominated by the jumping force during this short interval, whereas after the jump the ambient excitation governs the response and the bridge vibration is transferred to the pedestrian through the PSI mechanism.

Fig. 7 shows the acceleration response of the footbridge and the pedestrian. The amplitude of the vibrations increases due to the pedestrian's jumping, and the amplitude of the pedestrian response is slightly higher than that of the footbridge. The comparison of the frequency spectra of the footbridge and pedestrian responses is shown in Fig. 8a. The comparison with results of the standing case, shown in Fig. 4c and d, shows that the amplitude of the spectra at the first footbridge frequency increases significantly, while the amplitudes corresponding to the second and third frequencies remain nearly unchanged. This indicates that jumping primarily enhances the identification of the footbridge's first frequency. This behavior can be explained by the impulsive nature of the jumping load. Since the jump delivers a large impulsive input, it injects substantial energy into the interaction system and excites the global vibration of the footbridge more strongly than the ambient excitation alone. Because the first mode usually has the largest modal

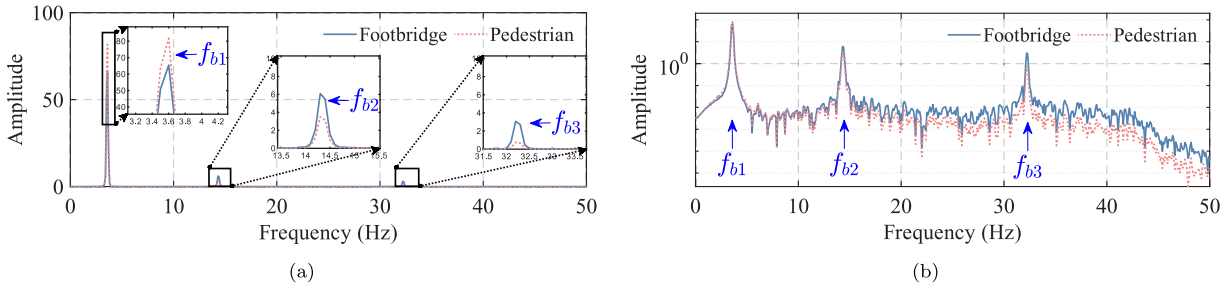

Fig. 8. Frequency spectra of the footbridge and jumping pedestrian: (a) linear scale; (b) log scale.

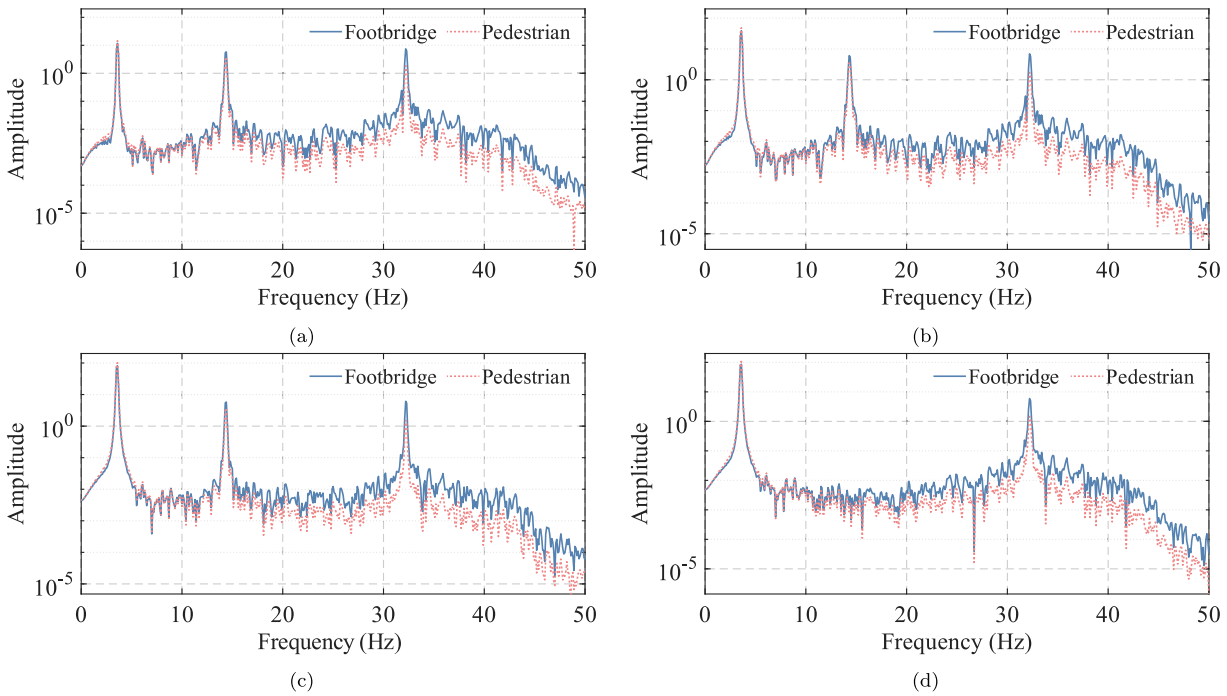

Fig. 9. Frequency spectra of the footbridge and jumping pedestrian at diverse positions: (a) jumping at $x = 3.3$ m; (b) jumping at $x = 6.6$ m; (c) jumping at $x = 13.2$ m; (d) jumping at $x = 16.5$ m.

participation and dominates the global vertical response, its spectral amplitude increases most significantly. By contrast, the higher modes remain less prominent in the pedestrian response due to their smaller modal participation and the attenuation effect introduced by the pedestrian dynamics.

Furthermore, as shown in Fig. 8b, when the pedestrian is jumping at $x = 9.9$ m, amplitude attenuation mainly occurs at frequencies above 10 Hz. To investigate the influence of jumping positions, cases were examined in which the pedestrian jumps at $x = 3.3$, 6.6, 13.2 m, and 16.5 m. The footbridge accelerations are recorded at the same positions. The results are shown in Fig. 9. The amplitude corresponding to the footbridge's fundamental frequency increases when the jumping position is close to the midpoint of the footbridge. Similar attenuation effects above 10 Hz can be observed regardless of the pedestrian's position. If $x = 16.5$ m, corresponding to the midpoint of the footbridge, the second natural frequency of the footbridge cannot be identified (Fig. 9d). These results indicate that the effectiveness of the jumping scenario depends on the modal amplitude at the jumping location. When the pedestrian jumps near an antinode of a given mode, the corresponding footbridge frequency becomes more visible in both the footbridge and pedestrian spectra. In contrast, when the jumping point is close to a modal node, the contribution of that mode is weak, and the corresponding frequency may become difficult to identify. This is why the second footbridge frequency is not visible when the jump occurs at the footbridge midpoint, which coincides with the node of the second mode for the simply supported beam model. Based on the above observations, using pedestrian response for footbridge frequency identification is particularly effective in the low-frequency range, such as below 10 Hz. The pedestrian acts like a "low-pass" filter that amplifies the spectral amplitude at the first footbridge frequency while attenuating those at the second and third frequencies. The identification of footbridge frequencies is not significantly affected, but the nodal points of the footbridge mode shapes should be avoided.

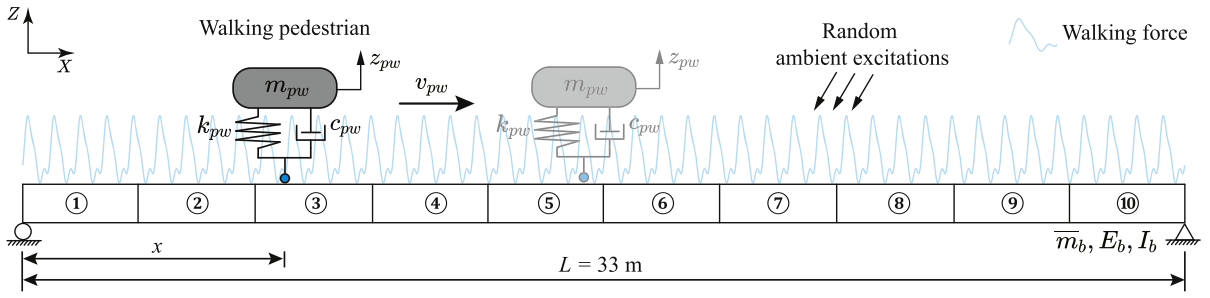

Fig. 10. Pedestrian walking on the footbridge.

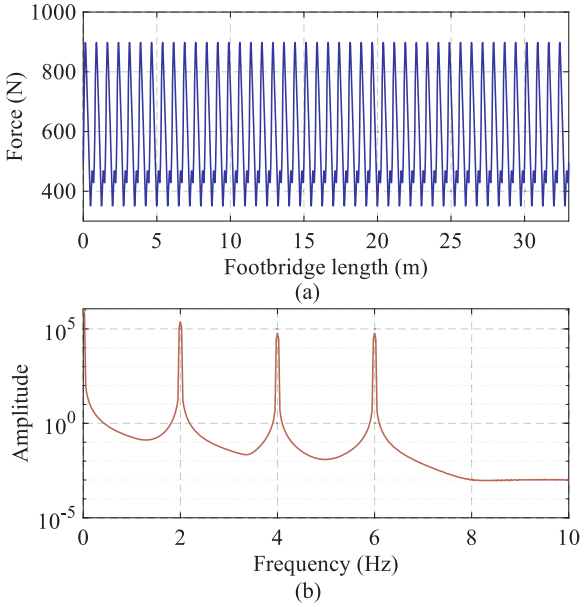

Fig. 11. Walking force and its spectrum: (a) walking force; (b) spectrum.

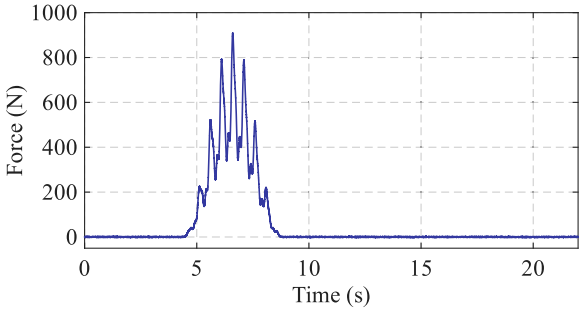

Fig. 12. Walking and ambient excitation at x = 9.9 m.

3.4. Scenario 3: walking/running

A common activity performed by pedestrians is walking or running on the footbridge. During the PSI process, the pedestrian excites the footbridge while simultaneously acting as a moving sensor that records its vibrations. Unlike Scenarios 1 and 2, the walking pedestrian moves across the entire length of the footbridge, continuously exciting it along the path, in addition to the ambient excitations. The model considered to simulate this scenario is shown in Fig. 10.

Using Eq. (4), the generated walking force without considering PSI and its corresponding frequency spectrum are shown in Fig. 11. When the pacing frequency is $f_{pw}^{p} = 2$ Hz and $n = 3$ harmonic components are considered in Eq. (4), the excitation consists

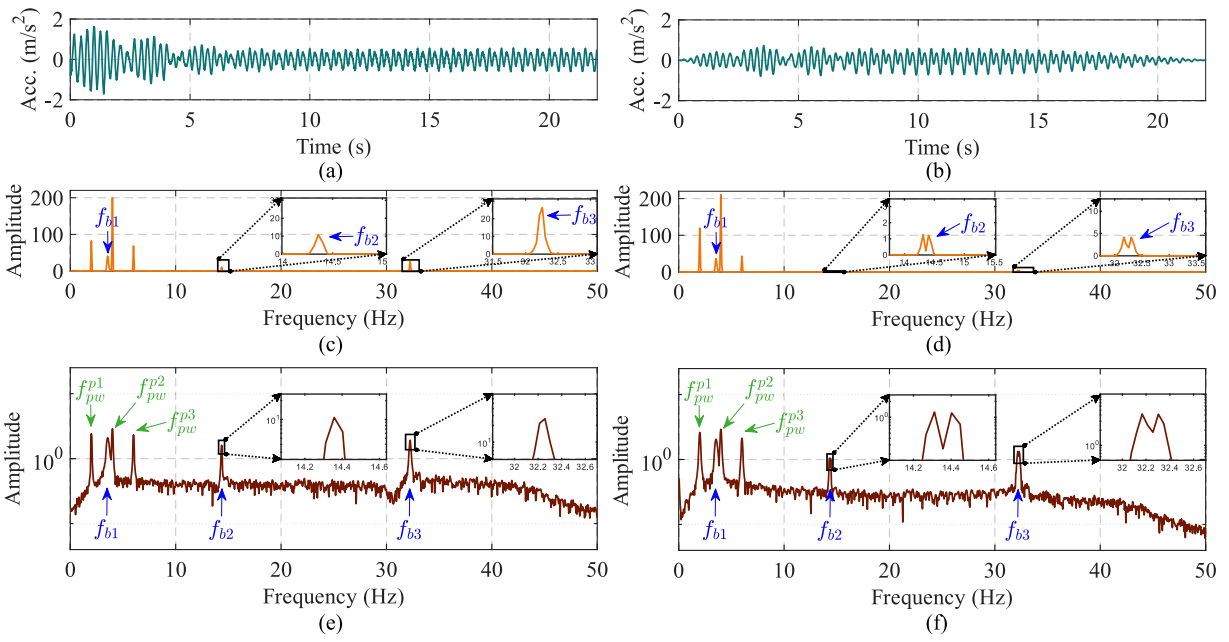

Fig. 13. Accelerations and frequency spectra of the footbridge and walking pedestrian: (a) footbridge acceleration; (b) pedestrian acceleration; (c) footbridge frequency spectrum in linear scale; (d) pedestrian frequency spectrum in linear scale; (e) footbridge frequency spectrum in log scale; (f) pedestrian frequency spectrum in log scale.

of three primary harmonic frequencies $f_{pw}^{p1} = 1f_{pw}^{p} = 2$ Hz, $f_{pw}^{p2} = 2f_{pw}^{p} = 4$ Hz, and $f_{pw}^{p3} = 3f_{pw}^{p} = 6$ Hz. As in the previous scenarios, the footbridge is divided into 10 elements. When the pedestrian is located between two nodes, the applied force is distributed to the adjacent nodes following the method described in Ref. [20]. For comparison with Scenario 2, the excitation applied to the footbridge at the point $x = 9.9$ m from the left end is shown in Fig. 12. The force reaches the peak value at time 6.604 s when the pedestrian is at location $x = 9.9$ m. The force is nearly zero during the time intervals $0 - 4.4$ s and $8.8 - 22$ s corresponding to the times when the pedestrian is at locations $x = 0 - 6.6$ m and $x = 13.2 - 33$ m. Its maximum amplitude is nevertheless smaller than that of the jumping force shown in Fig. 6. In addition, ambient excitations are also applied to all nodes of the footbridge's finite element model during the PSI process.

Fig. 13 shows the acceleration response and corresponding frequency spectra (in both linear and logarithmic scales) of the footbridge and the walking pedestrian. When the pedestrian walks across the footbridge, the acceleration response of the footbridge differs from that of the pedestrian, as they are measured at different locations on different subsystems. After a few seconds, the footbridge vibrations stabilize (between 5–22 s). For the pedestrian, however, the pedestrian's response amplitude reaches its maximum near the midpoint of the footbridge and decreases to nearly zero as the pedestrian approaches either end. The first three natural frequencies can be clearly identified from the frequency spectra of the footbridge. At the same time, the excitation frequencies f_{pw}^{p1}, f_{pw}^{p2}, and f_{pw}^{p3} corresponding to the pedestrian's harmonic pacing frequencies, are also observed, and their amplitudes are higher than those of the footbridge frequencies. A similar pattern is evident in the pedestrian's response frequency spectrum, where these excitation frequencies are also distinguishable. However, for the second and third footbridge frequencies, a "camel hump phenomenon" appears, characterized by two spectral peaks flanking the true bridge frequency. The "camel hump phenomenon" originates from the relative motion between the moving pedestrian and the vibrating footbridge, which causes a frequency modulation effect in the measured response. As demonstrated theoretically by Ref. [51], the dynamic response recorded by a moving sensor does not contain a single bridge resonance peak, but instead exhibits two sideband frequencies given by $f_{bn,l} = |f_{bn} - nv/(2L)|$ and $f_{bn,r} = |f_{bn} + nv/(2L)|$, where f_{bn} is the n-th bridge natural frequency, v is the moving speed, and L is the bridge span. These two frequencies correspond to the left and right peaks of the camel hump observed in the spectrum. Physically, this effect arises because the moving pedestrian samples the bridge vibration in a non-stationary manner. The bridge vibration is modulated by the pedestrian motion, leading to a split of the resonance energy into two adjacent frequency components that are symmetrically distributed around the true bridge frequency. As a result, the original bridge frequency does not appear as a single dominant peak, but as a trough between the two side peaks. Therefore, when the two peak frequencies of the camel hump are denoted as f_l and f_r, the bridge natural frequency can be reliably estimated as the midpoint between them, i.e., $f_{bn} = (f_{bn,l} + f_{bn,r})/2$. This interpretation is consistent with vehicle-based indirect frequency identification theory and explains why the camel hump becomes more pronounced at higher walking speeds and for higher bridge modes.

These results show that the footbridge information is well transferred to the walking pedestrian's response. When the bridge frequencies are close to the walking excitation frequencies, distinguishing them from pedestrian-induced harmonics in a single walking record may be difficult. However, when measurements from multiple pedestrians are available, walking harmonics are expected to

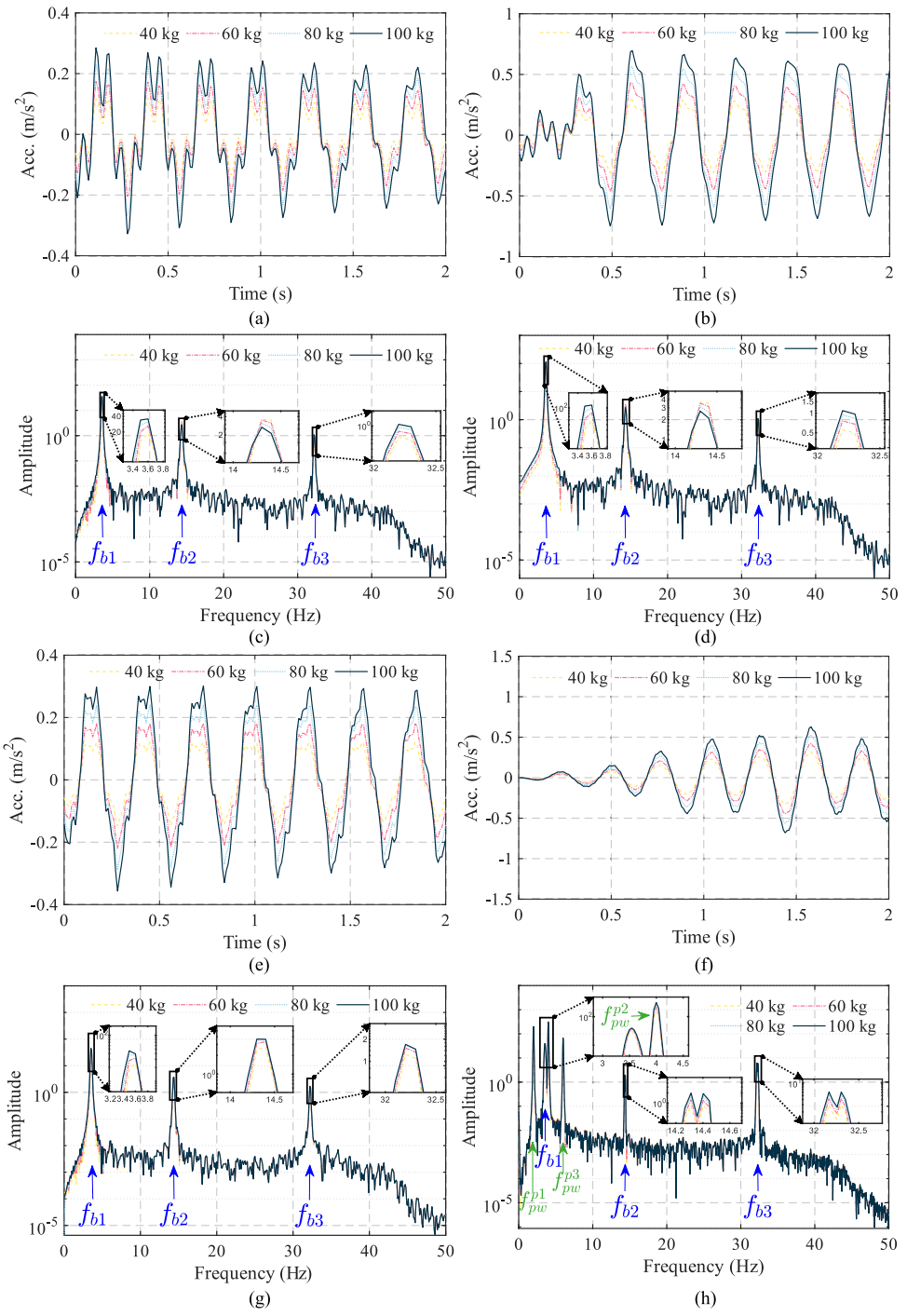

Fig. 14. Influence analysis of pedestrian weights: (a) accelerations of pedestrians standing at $x = 9.9$ m; (b) accelerations of pedestrians jumping at $x = 9.9$ m; (c) frequency spectra of pedestrians standing at $x = 9.9$ m; (d) frequency spectra of pedestrians jumping at $x = 9.9$ m; (e) accelerations of pedestrians standing at $x = 13.2$ m; (f) accelerations of walking pedestrians; (g) frequency spectra of pedestrians standing at $x = 13.2$ m; (h) frequency spectra of walking pedestrians.

vary due to differences in pacing frequency, whereas the bridge frequencies remain unchanged. Therefore, by combining spectra from multiple crossings, the consistent bridge frequencies can be more reliably identified. Another practical strategy is to first identify the pedestrian's walking frequencies from baseline measurements on a rigid surface (e.g., using the pedestrian response when they walk on the road) and then compare them with the footbridge-crossing spectra, so that the pedestrian-related spectral components can

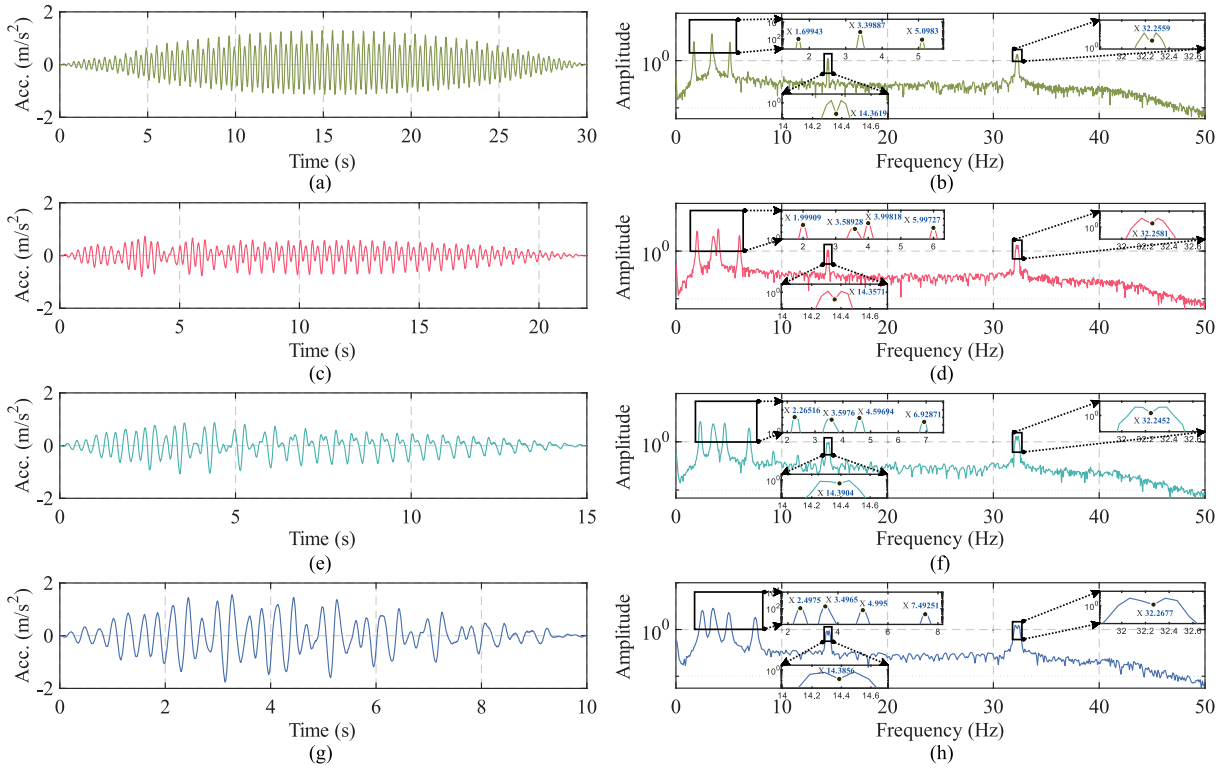

Fig. 15. Influence analysis of pedestrian walking speeds: (a) accelerations when v_{pw} = 1.1 m/s; (b) frequency spectra when v_{pw} = 1.1 m/s; (c) accelerations when v_{pw} = 1.5 m/s; (d) frequency spectra when v_{pw} = 1.5 m/s; (e) accelerations when v_{pw} = 2.2 m/s; (f) frequency spectra when v_{pw} = 2.2 m/s; (g) accelerations when v_{pw} = 3.3 m/s; (h) frequency spectra when v_{pw} = 3.3 m/s.

Table 3
Identified footbridge frequencies in different scenarios.

Activity	Identified bridge frequency (Hz)					
	f_{b1}	Error	f_{b2}	Error	f_{b3}	Error
True value	3.593	—	14.373	—	32.353	—
Scenario 1	3.545	1.34%	14.318	0.38%	32.227	0.39%
Scenario 2	3.545	1.34%	14.318	0.38%	32.227	0.39%
Scenario 3	3.544	1.36%	14.357	0.11%	32.235	0.36%

be distinguished from the bridge frequencies. In addition, when identifying the higher footbridge frequencies, the "camel hump phenomenon" must be considered.

Table 3 summarizes the results of footbridge frequency identification using the response of pedestrians performing different activities in the above scenarios. For the standing and jumping cases, 22 seconds of response data are analyzed to ensure the same frequency resolution as that of the walking response in Scenario 3. The errors in identifying the first three footbridge frequencies are within 2%, which is generally acceptable for engineering applications.

4. Parametric studies

In the previous section, numerical analysis demonstrated that footbridge natural frequencies can be successfully identified from the response of pedestrians. This section examines how pedestrian mass, walking speed, environmental noise, footbridge frequency, and structural damping affect the robustness of the proposed method. Unless otherwise specified, all other parameters are consistent with those adopted in Section 3.

4.1. Influence of pedestrian mass

Since body mass varies naturally across users in practical crowdsensing scenarios, it is important to examine whether such inter-person variability affects the transfer and identification of footbridge frequencies from pedestrian response. According to Ref. [52],

the average adult body mass worldwide is approximately 62 kg, although it varies across different countries. In this section, four pedestrian masses, namely 40 kg, 60 kg, 80 kg, and 100 kg, are analyzed. The corresponding acceleration response and frequency spectra of pedestrians performing different activities are presented in Fig. 14.

From the acceleration response shown in Fig. 14a and b, when pedestrians are standing and jumping on the footbridge, the vibration amplitude increases with the pedestrian mass. This increase can be partly attributed to the greater pedestrian-induced loading associated with heavier pedestrians; however, changes in pedestrian biodynamic properties may also influence the interaction and spectral transfer characteristics. A similar trend is evident in the response spectra shown in Fig. 14c and d, where the spectral amplitudes at the footbridge first and third modal frequencies (f_{b1} and f_{b3}) increase with the mass. However, the spectral amplitude at the second modal frequency f_{b2} decreases as the pedestrian mass increases. This occurs because the pedestrian is positioned at a fixed location on the footbridge. To further examine whether the amplitudes increase or decrease with pedestrian mass, additional positions were considered, namely $x = 3.3$ m, 6.6 m, and 13.2 m. When the pedestrian is standing at $x = 13.2$ m, the accelerations and frequency spectra of the pedestrians are shown in Fig. 14e and g. The results show that there is no consistent trend in the variation of spectral amplitudes with pedestrian mass, and this variation is not directly related to the footbridge mode shapes. Nevertheless, such changes in spectral amplitudes are associated with the pedestrian's standing/jumping positions. For the walking pedestrian, the increase in the pedestrian mass leads to a higher walking force, which in turn results in greater acceleration amplitudes, as shown in Fig. 14f. This increase is also reflected in the spectral amplitudes at both the walking frequencies (f_{pw}^{p1},f_{pw}^{p2}, and f_{pw}^{p3}) and the footbridge frequencies, as shown in Fig. 14h.

Overall, the influence of pedestrian mass on frequency identification is relatively limited within a realistic body-mass range, which suggests that the proposed method is reasonably robust to inter-person variability in practical applications.

4.2. Influence of pedestrian walking speed

Since walking or running is the most common activity of pedestrians on footbridges, it is important to further examine the effect of walking speed. In this section, the four walking speeds listed in Table 2 are considered, namely $v_{pw} = 1.1$, 1.5, 2.2, and 3.3 m/s. The acceleration responses of walking pedestrians at these four speeds, along with the corresponding frequency spectra, are shown in Fig. 15.

As the walking speed increases, the pedestrian's passing time on the footbridge becomes shorter, although the overall response shapes remain similar (Fig. 15a, c, e, and g). When the pedestrian walks slowly, three distinct peaks appear in the spectra (Fig. 15b) below 10 Hz, corresponding approximately to $f_{pw}^{p1} = 1.7$ Hz, $f_{pw}^{p2} = 3.4$ Hz, and $f_{pw}^{p3} = 5.1$ Hz. Under this condition, the second walking excitation component f_{pw}^{p2} is very close to the footbridge's first natural frequency $f_{b1} = 3.593$ Hz, thereby masking it and rendering the first footbridge frequency unidentifiable. However, the second and third footbridge frequencies, which are not influenced by the walking excitations, can still be identified with reasonable accuracy.

As the walking speed increases, the footbridge's first natural frequency becomes more distinguishable because the walking excitation frequencies shift farther away from it (Fig. 15d, f, and h). Another noticeable phenomenon is that the "camel hump phenomenon" becomes more pronounced, with a wider separation between the two peaks ($f_r - f_l$). Additionally, at higher walking speeds, the shorter passage duration results in a lower frequency resolution. For instance, when the walking speed reaches $v_{pw} = 3.3$ m/s, the identified first footbridge frequency is 3.4965 Hz, which is about 0.1 Hz lower than the true value. Therefore, relatively lower walking speeds can improve frequency resolution, provided that the walking harmonics do not overlap with the target footbridge frequencies.

4.3. Influence of environmental noise

In practical engineering applications, environmental noise is inevitably present in the acceleration measurement process. Therefore, in this section, simulated environmental noise is added to the pedestrian acceleration response. The contaminated signals can be represented by Eq. (10),

$$\mathbf{s}_c = \mathbf{s} + E_c \cdot N_s \cdot \sigma_s, \tag{10}$$

where $\mathbf{s}_c$ denotes the contaminated acceleration, $\mathbf{s}$ represents the original vibration response without environmental noise, and E_c indicates the noise level. N_s is a standard Gaussian random sequence with zero mean and unit variance, and σ_s is the standard deviation of the original acceleration. The contaminated pedestrian accelerations are then used for footbridge frequency identification. In this section, four levels of noise, 2%, 5%, 10%, and 20%, are considered. The pedestrian response acceleration signals during 0–5 s, considering 2% and 20% noise levels, are shown in Fig. 16 for various pedestrian activities. At low noise levels, the signal shape remains similar to that of the noise-free case. However, as the noise level increases, the acceleration values deviate more significantly from the noise-free signal, resulting in a more irregular pattern. The corresponding frequency spectra of the pedestrian response under different noise levels are presented in Fig. 17.

When the pedestrian is standing on the footbridge (Fig. 17a), the increase in the noise level makes the higher footbridge frequencies less identifiable. In particular, the third footbridge frequency becomes difficult to distinguish when the noise level reaches 20%; without prior knowledge, it is nearly impossible to identify it among the peaks. However, the first two footbridge frequencies remain identifiable, even though the frequency spectrum becomes more irregular.

As shown in Fig. 17b, the jumping force significantly amplifies the spectral amplitude at the footbridge's first natural frequency while reducing those at the second and third frequencies, with the third frequency becoming unidentifiable. When the pedestrian is walking (Fig. 17c), the second and third footbridge frequencies cannot be identified due to environmental noise interference.

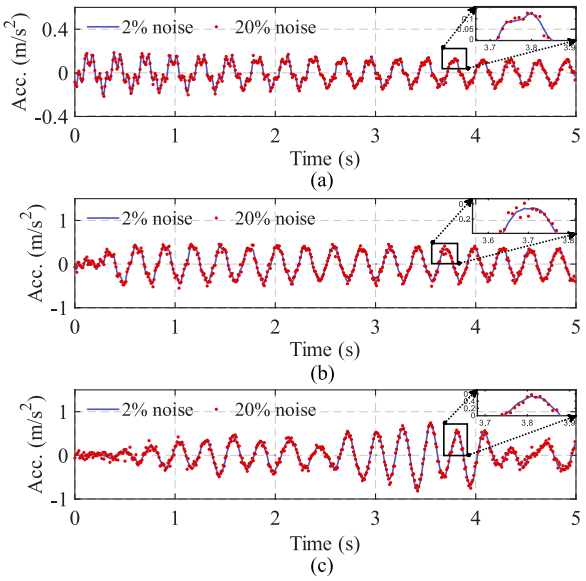

Fig. 16. Pedestrian response with environmental noise: (a) standing; (b) jumping; (c) walking.

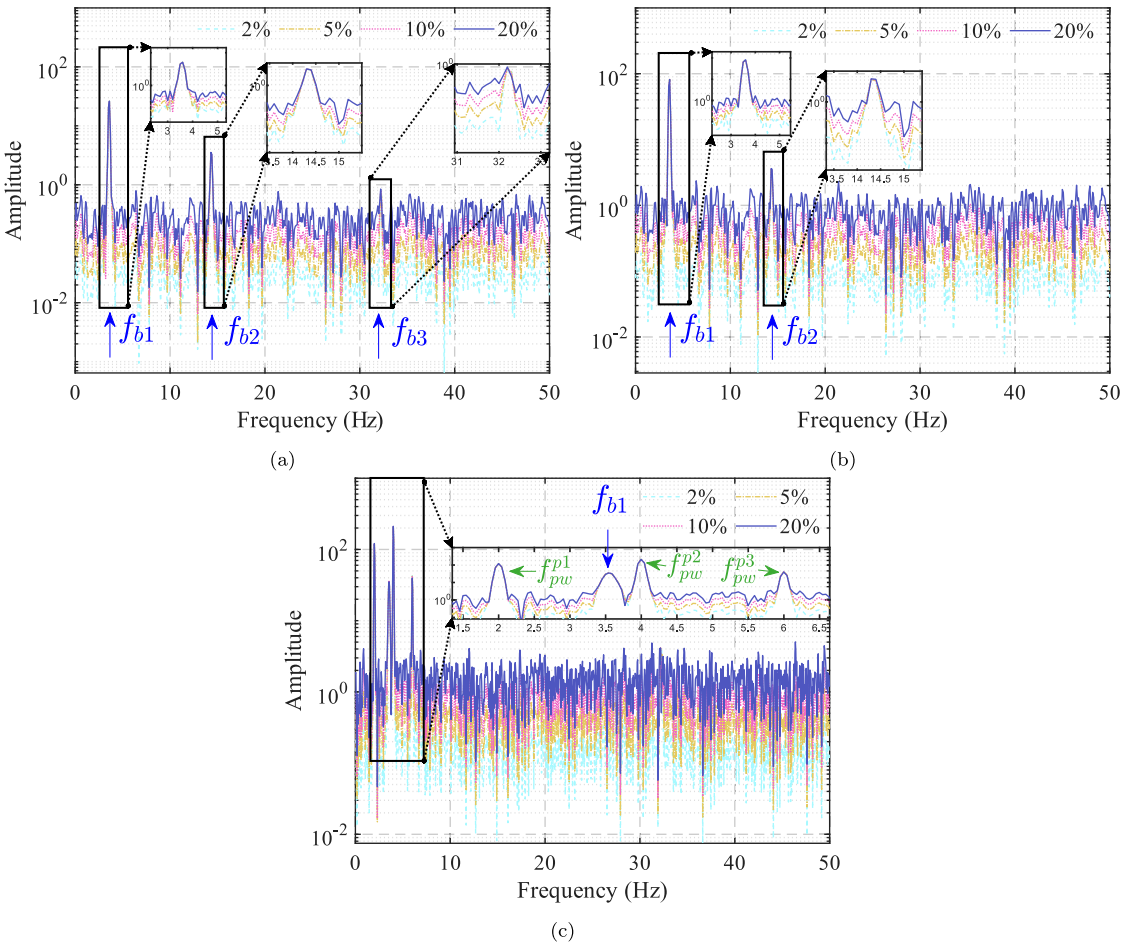

Fig. 17. Influence analysis of environmental noise: (a) standing pedestrian; (b) jumping pedestrian; (c) walking pedestrian.

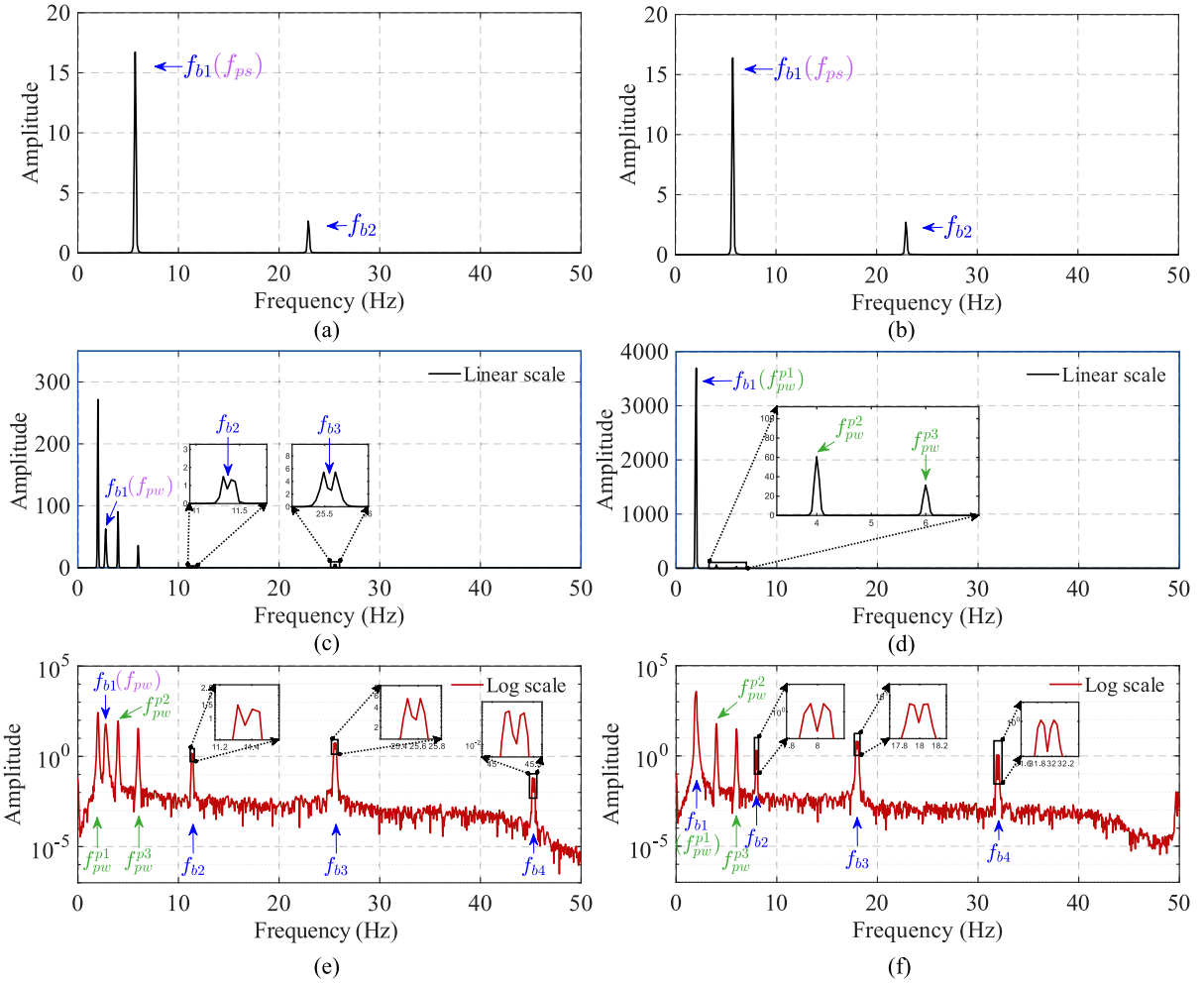

Fig. 18. Influence of footbridge frequency: (a) frequency spectrum of standing pedestrian in Case 1; (b) frequency spectrum of jumping pedestrian in Case 2; (c) linear-scale frequency spectrum of walking pedestrian in Case 3; (d) linear-scale frequency spectrum of walking pedestrian in Case 4; (e) log-scale frequency spectrum of walking pedestrian in Case 3; (f) log-scale frequency spectrum of walking pedestrian in Case 4.

Nevertheless, the walking excitation frequencies and the footbridge's fundamental frequency can still be observed. In such cases, the footbridge frequency needs to be extracted using alternative approaches.

Overall, environmental noise does not alter the spectral amplitudes at the footbridge frequencies but introduces additional spurious peaks. When the spectral amplitudes at certain footbridge frequencies (e.g., f_{b2} and f_{b3}) are relatively low, these additional peaks can obscure them, making their identification difficult. Furthermore, for walking pedestrians, part of the energy in the frequency spectrum is distributed to walking excitation frequencies, which further reduces the visibility of the higher footbridge modes. In other words, the signal-to-noise ratio (SNR) of the response from the standing and jumping pedestrians is higher than that from the walking pedestrian.

4.4. *Influence of footbridge frequency*

In engineering applications, resonance may occur when the natural frequencies of the structure are close to either the pedestrian's frequency or the pacing frequency [53]. To examine this issue, the influence of the bridge's natural frequency is investigated in this section. The footbridge natural frequencies are modified by changing the flexural stiffness $E_b I_b$, while keeping the mass per unit length $\overline{m}_b$ and span length L unchanged. Four cases, listed below, are considered. All other parameters remain the same as those used in Section 3. The corresponding frequency spectra are presented in Fig. 18.

- **Case 1:** Standing pedestrian frequency $f_{ps} = 5.741$ Hz. The footbridge flexural stiffness is $E_b I_b = 3.548 \times 10^9$ N · m^2, giving the first three footbridge frequencies $f_{b1} = 5.741$ Hz, $f_{b2} = 22.965$ Hz, and $f_{b3} = 51.693$ Hz.
- **Case 2:** Jumping pedestrian frequency $f_{ps} = 5.741$ Hz. The footbridge settings are the same as those in Case 1.

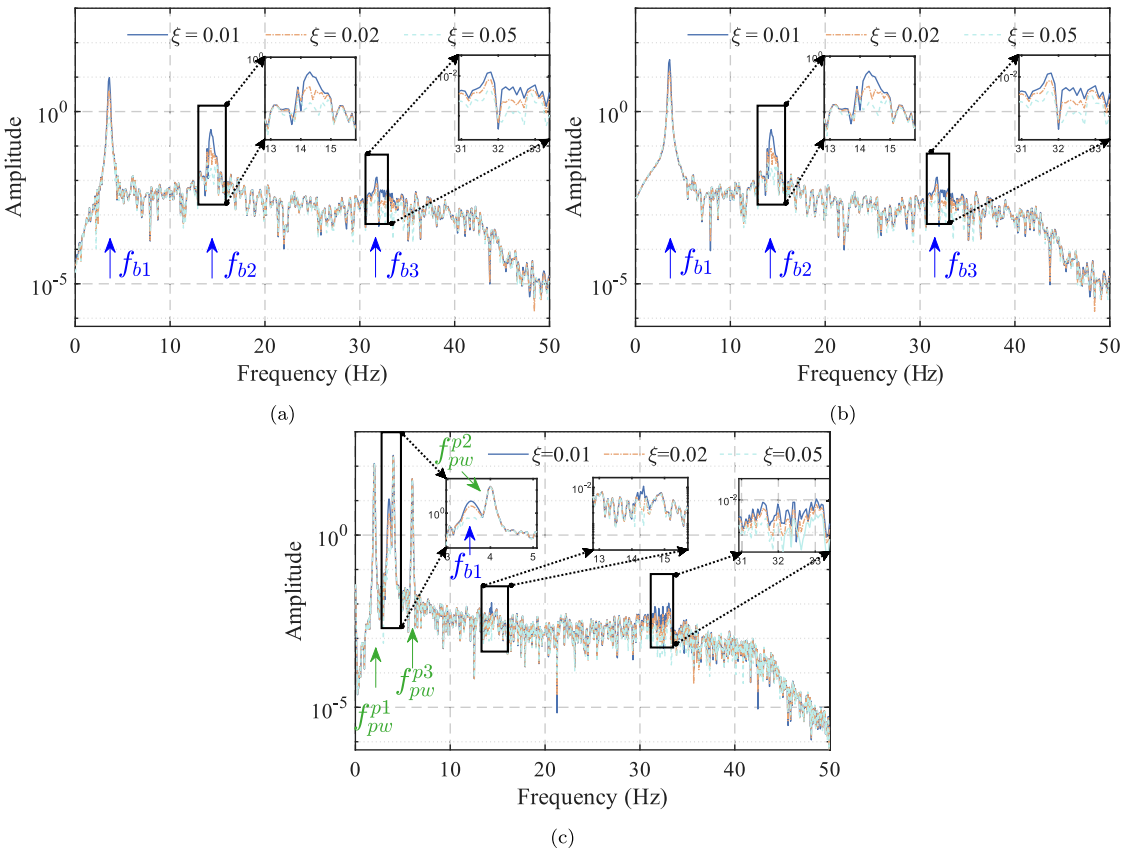

Fig. 19. Influence analysis of footbridge damping: (a) standing pedestrian; (b) jumping pedestrian; (c) walking pedestrian.

- **Case 3:** Walking pedestrian frequency $f_{pw} = 2.845$ Hz. The footbridge flexural stiffness is $E_b I_b = 8.711 \times 10^8$ N · m^2, giving the first three footbridge frequencies $f_{b1} = 2.845$ Hz, $f_{b2} = 11.379$ Hz, and $f_{b3} = 25.614$ Hz.
- **Case 4:** Walking pacing frequency $f_{pw}^{p} = 2.000$ Hz. The footbridge flexural stiffness is $E_b I_b = 4.307 \times 10^8$ N · m^2, giving the first three footbridge frequencies $f_{b1} = 2.000$ Hz, $f_{b2} = 8.001$ Hz, $f_{b3} = 18.010$ Hz.

As shown in Fig. 18a, when the fundamental frequency of the footbridge coincides with the standing pedestrian frequency in Case 1, the first two footbridge frequencies can still be clearly identified from the frequency spectrum of the standing pedestrian. Since the sampling frequency of the pedestrian response is 100 Hz, the third bridge frequency, $f_{b3} = 51.693$ Hz, cannot be identified because of the Nyquist sampling limit. A similar observation applies to Case 2. As shown in Fig. 18b, when the fundamental frequency of the footbridge coincides with that of the jumping pedestrian, the first two footbridge frequencies can also be identified clearly. For Case 3, where the footbridge fundamental frequency coincides with the walking pedestrian's frequency, the linear-scale frequency spectra shown in Fig. 18c indicates that the first three footbridge frequencies can still be identified. At the same time, the amplitude of f_{pw}^{p1} becomes larger than that of f_{pw}^{p2} when f_{b1} is close to f_{pw}^{p1}, which differs from the result shown in Fig. 13d, where the spectral amplitude of f_{pw}^{p2} is larger because f_{b1} is close to f_{pw}^{p2}. In addition, as in Scenario 3 described in Section 3.4, the walking excitation frequencies can also be identified from the spectrum. To present the spectral peaks more clearly, the results are also plotted on a logarithmic scale, as shown in Fig. 18e. The "camel hump phenomenon" still exists at the higher frequencies. Therefore, the above results indicate that frequency coincidence between the footbridge and the pedestrian natural frequencies does not significantly hinder footbridge frequency identification.

For Case 4, where the footbridge fundamental frequency coincides with the pacing frequency, the frequency-identification results are shown in Fig. 18d and f. From the linear-scale spectrum, the spectral amplitude at the footbridge's fundamental frequency is greatly amplified due to resonance between the pedestrian pacing frequency and the footbridge frequency. Because of this amplification, the other two walking excitation frequencies, f_{pw}^{p2} and f_{pw}^{p3}, become less prominent. To show all spectral peaks more clearly, the results are also plotted on a log scale. Even when the footbridge fundamental frequency coincides with the pacing frequency, the higher footbridge frequencies can still be identified, although the "camel hump phenomenon" remains present. However, identification of the footbridge fundamental frequency becomes challenging because the two frequencies overlap. In such cases, additional measures may be needed. In practical crowdsensing applications, the proposed method is not intended to use a single pedestrian signal alone, but to combine responses from multiple pedestrians with different pacing frequencies. Such joint processing can reduce the influence

of individual pacing characteristics and improve the reliability of footbridge frequency identification. Prior estimation of the pacing frequency before the pedestrian enters the footbridge may also be helpful.

4.5. Influence of footbridge damping

Damping of the footbridge is another important factor influencing its dynamic behavior. In this study, Rayleigh damping is adopted, where the damping ratios of the first two modes are assumed to be equal, i.e., $\xi = \xi_1 = \xi_2$. The coefficients α_0 and β_0 in $\mathbf{C} = \alpha_0\mathbf{M} + \beta_0\mathbf{K}$ are then determined accordingly. This section investigates three values of the damping ratio, namely $\xi = 0.01$, $\xi = 0.02$, and $\xi = 0.05$, which are typical values used for bridges [54,55]. The corresponding frequency spectra of the pedestrian response are presented in Fig. 19.

From Fig. 19a and b, when the damping ratio is relatively low (i.e. $\xi = 0.01$), the first three footbridge frequencies remain identifiable. Furthermore, increasing the damping ratio leads to a reduction in the amplitudes of all footbridge frequencies. This trend is similar to the effect observed in Section 4.1 for a lighter pedestrian mass. However, the underlying mechanisms differ. A lighter pedestrian mass weakens the pedestrian–footbridge interaction, reducing the energy transferred from the pedestrian to the structure. In contrast, a higher damping ratio means that the footbridge itself dissipates more energy through damping, resulting in lower vibration amplitudes.

For the case of a walking pedestrian (Fig. 19c), increasing the footbridge damping also makes the “camel hump phenomenon” less pronounced, which may further increase the difficulty of identifying higher footbridge frequencies. When $\xi = 0.01$ and $\xi = 0.02$, the fundamental frequency of the footbridge remains identifiable, while the higher modes are overshadowed. Moreover, the damping effect is only evident in the amplitudes associated with the footbridge frequencies, while the walking excitation frequencies remain unaffected. When the damping ratio increases to $\xi = 0.05$, the fundamental frequency becomes unidentifiable. Under such conditions, stronger excitations are required to effectively stimulate the footbridge, such as those generated by an external shaker or by multiple pedestrians walking simultaneously, as demonstrated in existing studies on indirect road bridge monitoring [56–58].

5. Conclusions and future studies

This paper proposes a pedestrian-response-based method for identifying footbridge natural frequencies, with direct relevance to crowdsensing-based structural health monitoring. Three pedestrian activities, standing, jumping, and walking, are analyzed to achieve effective indirect identification of footbridge frequencies. Furthermore, the effects of key parameters, including pedestrian mass, walking speed, environmental noise, footbridge frequency, and footbridge damping, are examined. The main conclusions can be summarized as follows:

(i) When standing, the footbridge frequencies can be clearly identified from pedestrian response, even under purely random ambient excitations. The pedestrian’s own frequency does not appear in the spectrum due to the high damping of the standing pedestrian, which helps highlight the footbridge frequencies.
(ii) When jumping, compared with the footbridge response spectrum, the pedestrian acts as a weak “low-pass filter” that amplifies the first footbridge frequency while attenuating the amplitudes of the second and third frequencies.
(iii) When the walking pedestrian’s response is employed, the walking excitation frequencies become identifiable in the pedestrian response spectrum, and a “camel hump phenomenon” appears for the higher footbridge frequencies.
(iv) Pedestrian mass has a minor influence on the identified footbridge spectral amplitudes owing to the limited variation in body mass across individuals.
(v) A higher walking speed enhances the “camel hump phenomenon” and reduces frequency resolution, thereby lowering identification accuracy.
(vi) Environmental noise mainly affects high-frequency bands and hinders the identification of higher footbridge frequencies from the pedestrian response.
(vii) Coincidence between the footbridge frequency and the pedestrian natural frequency does not significantly hinder footbridge frequency identification, whereas coincidence with the pacing frequency can hinder the identification of the corresponding resonant footbridge frequency.
(viii) Higher footbridge damping attenuates the spectral amplitudes, thereby reducing the identification reliability of footbridge frequencies.

Although the numerical results are encouraging, several factors relevant to real-world applications, including multiple simultaneous pedestrians and temperature-induced frequency variations, have not been addressed. The findings regarding information transfer from the footbridge to pedestrians lay the groundwork for crowdsensing-based footbridge health monitoring. The proposed method should be regarded as a complementary screening tool for footbridges rather than a substitute for conventional bridge-mounted sensing. Its practical value lies in enabling opportunistic data collection from pedestrians carrying smartphones or wearable devices during normal bridge usage. Prior to deployment in crowdsensing applications, the method requires validation through laboratory experiments and field tests. Future work will focus on examining the effects of these additional factors and conducting further demonstration studies in real engineering environments.

CRediT authorship contribution statement

Zhenkun Li: Writing – original draft, Visualization, Resources, Methodology, Formal analysis, Conceptualization; **Suzana Ereiz:** Writing – review & editing, Formal analysis; **Ekin Ozer:** Writing – review & editing, Conceptualization; **Abdollah Malekjafarian:** Writing – review & editing, Methodology; **Maria Pina Limongelli:** Writing – review & editing, Supervision.

Data availability

Data will be made available on request.

Declaration of competing interest

The authors declare that they have no known competing financial interests or personal relationships that could have appeared to influence the work reported in this paper.

Acknowledgements

Z. Li acknowledges the support of the MSCA Seal of Excellence research fellowship funded by Politecnico di Milano. E. Ozer acknowledges the financial support of Science Foundation Ireland under grant number 22/FFP-P/11577. M.P. Limongelli carried out this study within the RETURN Extended Partnership and received funding from the European Union Next-GenerationEU (National Recovery and Resilience Plan – NRRP, Mission 4, Component 2, Investment 1.3 – D.D. 1243 2/8/2022, PE0000005).

References

[1] P. Negi, R. Kromanis, A.G. Dorée, K.M. Wijnberg, Structural health monitoring of inland navigation structures and ports: a review on developments and challenges, Struct. Health Monit. 23 (1) (2023) 605–645. https://doi.org/10.1177/14759217231170742
[2] European Commission, Joint Research Centre, K. Gkoumas, M. Balen, M. Grosso, F. Pekár, F. Marques Dos Santos, G. Haq, A. Ortega Hortelano, A. Tsakalidis, Research and innovation in bridge maintenance, inspection and monitoring : a European perspective based on the Transport Research and Innovation Monitoring and Information System (TRIMIS), Publications Office, 2019. https://doi.org/10.2760/16174
[3] American Society of Civil Engineers, ASCE's 2021 infrastructure report card: bridges, https://infrastructurereportcard.org/wp-content/uploads/2020/12/Bridges-2021.pdf. 2021 (accessed 15 January 2026).
[4] X. An, J. Hou, Ł. Jankowski, Q. Zhang, A physics-augmented deep learning framework for structural dynamic load identification with FRF-guided state expansion, Mech. Syst. Signal Process. 247 (2026) 113965. https://doi.org/10.1016/j.ymssp.2026.113965
[5] Y. Fu, Z. Wang, A. Maghareh, S. Dyke, M. Jahanshahi, A. Shahriar, F. Zhang, Effective structural impact detection and localization using convolutional neural network and Bayesian information fusion with limited sensors, Mech. Syst. Signal Process. 224 (2025) 112074. https://doi.org/10.1016/j.ymssp.2024.112074
[6] M.P. Limongelli, P.F. Giordano, Vibration-based damage indicators: a comparison based on information entropy, J. Civ. Struct. Health Monit. 10 (2) (2020) 251–266. https://doi.org/10.1007/s13349-020-00381-9
[7] Y. Zhang, Z. Li, R. Hao, W. Lin, L. Li, D. Su, High-fidelity time-series data synthesis based on finite element simulation and data space mapping, Mech. Syst. Signal Process. 200 (2023) 110630. https://doi.org/10.1016/j.ymssp.2023.110630
[8] Y. An, E. Chatzi, S.H. Sim, S. Laflamme, B. Blachowski, J. Ou, Recent progress and future trends on damage identification methods for bridge structures, Struct. Control Health Monit. 26 (10) (2019) e2416. https://doi.org/10.1002/stc.2416
[9] Z. Wang, D.H. Yang, T.H. Yi, G.H. Zhang, J.G. Han, Eliminating environmental and operational effects on structural modal frequency: A comprehensive review, Struct. Control Health Monit. 29 (11) (2022) e3073. https://doi.org/10.1002/stc.3073
[10] Z. He, W. Li, H. Salehi, H. Zhang, H. Zhou, P. Jiao, Integrated structural health monitoring in bridge engineering, Autom. Constr. 136 (2022) 104168. https://doi.org/10.1016/j.autcon.2022.104168
[11] A. Malekjafarian, R. Corbally, W. Gong, A review of mobile sensing of bridges using moving vehicles: progress to date, challenges and future trends, Structures 44 (2022) 1466–1489. https://doi.org/10.1016/j.istruc.2022.08.075
[12] Z. Li, W. Lin, C.-W. Kim, M.P. Limongelli, E. Chatzi, A comprehensive review of indirect bridge health monitoring, Mech. Syst. Signal Process. 247 (2026) 113918. https://doi.org/10.1016/j.ymssp.2026.113918
[13] L.A. Bull, P.A. Gardner, J. Gosliga, T.J. Rogers, N. Dervilis, E.J. Cross, E. Papatheou, A.E. Maguire, C. Campos, K. Worden, Foundations of population-based SHM, Part I: Homogeneous populations and forms, Mech. Syst. Signal Process. 148 (2021) 107141. https://doi.org/10.1016/j.ymssp.2020.107141
[14] Z. Li, Y. Lan, W. Lin, Footbridge damage detection using smartphone-recorded responses of micromobility and convolutional neural networks, Autom. Constr. 166 (2024) 105587. https://doi.org/10.1016/j.autcon.2024.105587
[15] H. Qiao, H. Guan, Y. Zhu, Footbridge structural health monitoring – A review of current research and future directions, Struct. Infrastruct. Eng. 0 (0) (2025) 1–24. https://doi.org/10.1080/15732479.2025.2547349
[16] C.W. Kim, M. Kawatani, Challenge for a drive-by bridge inspection, in: 10th International Conference on Safety, Reliability and Risk of Structures, Infrastructures and Engineering Systems, Osaka, Japan, 13–17 September, 2009, CRC Press, 2009, p. 758–765. https://doi.org/10.1201/9780367803667
[17] H. Xu, X.Y. Chen, J. Chen, L.K. Shi, D.S. Yang, Z.L. Wang, Y.B. Yang, Review of vehicle scanning method for bridges from 2004 to 2024, Int. J. Struct. Stab. Dyn. 25 (19) (2024) 2530003. https://doi.org/10.1142/S0219455425300034
[18] Y.B. Yang, C.W. Lin, J.D. Yau, Extracting bridge frequencies from the dynamic response of a passing vehicle, J. Sound Vib. 272 (3) (2004) 471–493. https://doi.org/10.1016/S0022-460X(03)00378-X
[19] C.W. Lin, Y.B. Yang, Use of a passing vehicle to scan the fundamental bridge frequencies: an experimental verification, Eng. Struct. 27 (13) (2005) 1865–1878. https://doi.org/10.1016/j.engstruct.2005.06.016
[20] Z. Li, Y. Lan, W. Lin, Indirect damage detection for bridges using sensing and temporarily parked vehicles, Eng. Struct. 291 (2023) 116459. https://doi.org/10.1016/j.engstruct.2023.116459
[21] R. Corbally, A. Malekjafarian, Experimental verification of a data-driven algorithm for drive-by bridge condition monitoring, Struct. Infrastruct. Eng. 20 (7-8) (2024) 1174–1196. https://doi.org/10.1080/15732479.2024.2311902
[22] C. Liu, Y. Zhu, H. Ye, Bridge frequency identification based on relative displacement of axle and contact point using tire pressure monitoring, Mech. Syst. Signal Process. 183 (2023) 109613. https://doi.org/10.1016/j.ymssp.2022.109613
[23] S. Cafiso, A. Di Graziano, V. Marchetta, G. Pappalardo, Urban road pavements monitoring and assessment using bike and e-scooter as probe vehicles, Case Stud. Constr. Mater. 16 (2022) e00889. https://doi.org/10.1016/j.cscm.2022.e00889

[24] P.F. Giordano, S. Quqa, M.P. Limongelli, Lightweight vehicles in indirect structural health monitoring: Current advances and future prospects, in: Bridge Maintenance, Safety, Management, Digitalization and Sustainability, CRC Press, Boca Raton, FL, USA, 2024, pp. 3441–3449. https://doi.org/10.1201/9781003483755-407
[25] S. Quqa, P.F. Giordano, M.P. Limongelli, Shared micromobility-driven modal identification of urban bridges, Autom. Constr. 134 (2022) 104048. https://doi.org/10.1016/j.autcon.2021.104048
[26] R. May, H.K. Chai, T. Reynolds, Y. Lu, Field investigation of bicycles for indirect bridge structural health monitoring, J. Civ. Struct. Health Monit. 15 (2024) 465–481. https://doi.org/10.1007/s13349-024-00885-8
[27] N. McSweeney, R. Ghiasi, A. Malekjafarian, E. Ozer, Extracting bridge modal frequencies using stationary versus drive-by modes of smartphone measurements, Infrastructures 9 (12) (2024) 218. https://doi.org/10.3390/infrastructures9120218
[28] L. Wang, S. Nagarajaiah, W. Shi, Y. Zhou, Semi-active control of walking-induced vibrations in bridges using adaptive tuned mass damper considering human-structure-interaction, Eng. Struct. 244 (2021) 112743. https://doi.org/10.1016/j.engstruct.2021.112743
[29] L. Wang, S. Nagarajaiah, Y. Zhou, W. Shi, Experimental study on adaptive-passive tuned mass damper with variable stiffness for vertical human-induced vibration control, Eng. Struct. 280 (2023) 115714. https://doi.org/10.1016/j.engstruct.2023.115714
[30] L. Wang, Y. Zhou, W. Shi, Random crowd-induced vibration in footbridge and adaptive control using semi-active TMD including crowd-structure interaction, Eng. Struct. 306 (2024) 117839. https://doi.org/10.1016/j.engstruct.2024.117839
[31] E. Ozer, M.Q. Feng, Biomechanically influenced mobile and participatory pedestrian data for bridge monitoring, Int. J. Distrib. Sens. Netw. 13 (4) (2017) 1550147717705240. https://doi.org/10.1177/1550147717705240
[32] Z. Wang, V. Ramamoorthy, U. Gal, A. Guez, Possible life saver: A review on human fall detection technology, Robotics 9 (3) (2020) 55. https://doi.org/10.3390/robotics9030055
[33] M. Straczkiewicz, P. James, J.-P. Onnela, A systematic review of smartphone-based human activity recognition methods for health research, npj Digit. Med. 4 (148) (2021) 1–15. https://doi.org/10.1038/s41746-021-00514-4
[34] E. Ozer, M.Q. Feng, D. Feng, Citizen sensors for SHM: Towards a crowdsourcing platform, Sensors 15 (6) (2015) 14591–14614. https://doi.org/10.3390/s150614591
[35] H. Sarmadi, A. Entezami, K.V. Yuen, B. Behkamal, Review on smartphone sensing technology for structural health monitoring, Measurement 223 (2023) 113716. https://doi.org/10.1016/j.measurement.2023.113716
[36] E. Ozer, R. Kromanis, Smartphone prospects in bridge structural health monitoring, a literature review, Sensors 24 (11) (2024) 3287. https://doi.org/10.3390/s24113287
[37] Y. Matsumoto, M.J. Griffin, Mathematical models for the apparent masses of standing subjects exposed to vertical whole-body vibration, J. Sound Vib. 260 (3) (2003) 431–451. https://doi.org/10.1016/S0022-460X(02)00941-0
[38] V. Racic, A. Pavic, Mathematical model to generate near-periodic human jumping force signals, Mech. Syst. Signal Process. 24 (1) (2010) 138–152. https://doi.org/10.1016/j.ymssp.2009.07.001
[39] M.A. Toso, H.M. Gomes, F.T. Da Silva, R.L. Pimentel, Experimentally fitted biodynamic models for pedestrian-structure interaction in walking situations, Mech. Syst. Signal Process. 72-73 (2016) 590–606. https://doi.org/10.1016/j.ymssp.2015.10.029
[40] F.T. da Silva, H.M. B.F. Brito, R.L. Pimentel, Modeling of crowd load in vertical direction using biodynamic model for pedestrians crossing footbridges, Can. J. Civ. Eng. 40 (12) (2013) 1196–1204. https://doi.org/10.1139/cjce-2011-0587
[41] H. Bachmann, W.J. Ammann, F. Deischl, J. Eisenmann, I. Floegl, G.H. Hirsch, G.K. Klein, G.J. Lande, O. Mahrenholtz, H.G. Natke, et al., Vibration problems in structures: practical guidelines, Springer Science & Business Media, 1995.
[42] J. Máca, J. Stepánek, Pedestrian load models of footbridges, MATEC Web Conf. 107 (2017) 00009. https://doi.org/10.1051/matecconf/201710700009
[43] Z. Li, W. Lin, Y. Zhang, Bridge frequency scanning using the contact-Point response of an instrumented 3D vehicle: Theory and numerical simulation, Struct. Control Health Monit. 2023 (2023) 3924349. https://doi.org/10.1155/2023/3924349
[44] Z. Li, Y. Lan, W. Lin, Indirect frequency identification of footbridges with pedestrians using the contact-Point response of shared scooters, J. Bridge Eng. 29 (6) (2024) 04024036. https://doi.org/10.1061/JBENF2.BEENG-6344
[45] A. González, Vehicle-bridge dynamic interaction using finite element modelling, INTECH Open Access Publisher, 2010.
[46] R.W. Clough, J. Penzien, Dynamics of Structures, McGraw-Hill College, 1975.
[47] A. González, E. Covián, M. Casero, Verifying the suitability of uncoupled numerical methods for solving vehicle-bridge interaction problems, Struct. Infrastruct. Eng. 19 (10) (2023) 1407–1424. https://doi.org/10.1080/15732479.2022.2033276
[48] C.C. Caprani, E. Ahmadi, Formulation of human–structure interaction system models for vertical vibration, J. Sound Vib. 377 (2016) 346–367. https://doi.org/10.1016/j.jsv.2016.05.015
[49] K. Van Nimmen, G. Lombaert, G. De Roeck, P. Van den Broeck, The impact of vertical human-structure interaction on the response of footbridges to pedestrian excitation, J. Sound Vib. 402 (2017) 104–121. https://doi.org/10.1016/j.jsv.2017.05.017
[50] A. Cunha, R. Sampaio, On the nonlinear stochastic dynamics of a continuous system with discrete attached elements, Appl. Math. Model. 39 (2) (2015) 809–819. https://doi.org/10.1016/j.apm.2014.07.012
[51] Z. Shi, N. Uddin, Extracting multiple bridge frequencies from test vehicle – a theoretical study, J. Sound Vib. 490 (2021) 115735. https://doi.org/10.1016/j.jsv.2020.115735
[52] S.C. Walpole, D. Prieto-Merino, P. Edwards, J. Cleland, G. Stevens, I. Roberts, The weight of nations: an estimation of adult human biomass, BMC Public Health 12 (2012) 439. https://doi.org/10.1186/1471-2458-12-439
[53] L. Wang, Y. Zhou, W. Shi, Dynamic test, monitoring and active control of non-resonant running-induced vibration for floor structure, Structures 63 (2024) 106348. https://doi.org/10.1016/j.istruc.2024.106348
[54] A. González, E.J. OBrien, P.J. McGetrick, Identification of damping in a bridge using a moving instrumented vehicle, J. Sound Vib. 331 (18) (2012) 4115–4131. https://doi.org/10.1016/j.jsv.2012.04.019
[55] Y.B. Yang, B. Zhang, Y. Chen, Y. Qian, Y. Wu, Bridge damping identification by vehicle scanning method, Eng. Struct. 183 (2019) 637–645. https://doi.org/10.1016/j.engstruct.2019.01.041
[56] Y.B. Yang, C.C. Huang, H. Xu, M.H. Wang, Z.L. Wang, K. Shi, Frequency extraction for bridges with rough surface by a moving test vehicle enhanced by a shaker, Eng. Struct. 266 (2022) 114598. https://doi.org/10.1016/j.engstruct.2022.114598
[57] Z. Hu, Z. Xiang, Damage detection for continuous beams by using the tap-scan method, Appl. Math. Model. 135 (2024) 524–540. https://doi.org/10.1016/j.apm.2024.07.007
[58] J. Zhang, T.H. Yi, C.X. Qu, Q. Han, Y.F. Wang, X.D. Mei, Experimental studies of extracting bridge mode shapes by response of a moving vehicle, J. Bridge Eng. 28 (11) (2023) 04023076. https://doi.org/10.1061/JBENF2.BEENG-6243